Check for updates

RESEARCH ARTICLE

REVISED On elastic deformations of cylindrical bodies under the influence of the gravitational field

[version 2; peer review: 3 approved, 1 approved with reservations]

Hamed Barzegar[1], Piotr T. Chruściel[2], Elisabeth Steininger[2]

[1]Centre de Recherche Astrophysique de Lyon, Universite Claude Bernard Lyon 1, Villeurbanne, Auvergne-Rhône-Alpes, 69622, France
[2]Faculty of Physics, University of Vienna, Vienna, Vienna, 1090, Austria

v2 **First published:** 10 May 2024, **4**:98
https://doi.org/10.12688/openreseurope.17329.1
Latest published: 04 Dec 2024, **4**:98
https://doi.org/10.12688/openreseurope.17329.2

Abstract

Background

Elastic deformations of gravitating cylindrical bodies are relevant for state-of-the-art photonic experiments, as they affect the physical properties of materials under consideration, impacting wave propagation. This is of key importance for a recently planned experiment to explore the influence of the gravitational field on entangled photons propagating in waveguides. The purpose of this work is to determine these elastic deformations as functions of temperature, pressure, and of the gravitational field. We thus determine the deformations of the body due to changes of the gravitational field, and obtain stringent bounds on the control of temperature and pressure so that the effects of the associated elastic deformations on the photons propagating in a waveguide are smaller than the phase shifts associated with the change of the gravitational field.

Methods

We use the methods of linear elasticity, including thermoelasticity, to determine the stresses and strains of the medium. For this, the symmetry of the cylinder allows us to solve the problem by using Mitchell's solutions of the equations satisfied by the Airy functions. The boundary conditions are implemented by an approximation of the Hertz contact method.

Results

Open Peer Review

Approval Status ✓ ✓ ? ✓

	1	2	3	4
version 2 (revision) 04 Dec 2024		✓ view		✓ view
version 1 10 May 2024	✓ view	? view	? view	

1. **Robert Beig**, Universitat Wien, Vienna, Austria
2. **Matthew Maitra**, ETH Zurich, Zürich, Switzerland
3. **Michele Brun**, University of Cagliari, Cagliari, Italy
4. **Ilya Svetlizky**, Technion Israel Institute of Technology (Ringgold ID: 26747), Haifa, Israel

Any reports and responses or comments on the article can be found at the end of the article.

We calculate the displacements, the stresses and strains for several classes of boundary conditions, and give explicit solutions for a number of physically motivated configurations. The influence of the resulting deformations on the planned GRAVITES experiment is determined.

Conclusions

The results are relevant for fiber interferometry experiments sensitive to the effects of the gravitational field on photon propagation. Our calculations give stringent bounds on the environmental variables, which need to be controlled in such experiments.

Keywords
linear elasticity, GRAVITES, waveguides, Airy stress, Michell solution

This article is included in the Horizon Europe gateway.

This article is included in the European Research Council (ERC) gateway.

This article is included in the Horizon 2020 gateway.

Corresponding author: Elisabeth Steininger (elisabeth.steininger@univie.ac.at)

Author roles: Barzegar H: Conceptualization, Formal Analysis, Validation, Visualization, Writing – Original Draft Preparation, Writing – Review & Editing; **Chruściel PT**: Conceptualization, Funding Acquisition, Methodology, Project Administration, Resources, Supervision, Validation, Writing – Original Draft Preparation, Writing – Review & Editing; **Steininger E**: Conceptualization, Data Curation, Formal Analysis, Investigation, Methodology, Software, Visualization, Writing – Original Draft Preparation, Writing – Review & Editing

Competing interests: No competing interests were disclosed.

Grant information: This project has received funding from the European Research Council (ERC) under the European Union's Horizon 2020 research and innovation programme (Grant agreement No. 740021), and under the Horizon Europe Framework Programme [101071779] and the Austrian Science Fund [P34274].
The funders had no role in study design, data collection and analysis, decision to publish, or preparation of the manuscript.

Copyright: © 2024 Barzegar H *et al*. This is an open access article distributed under the terms of the Creative Commons Attribution License, which permits unrestricted use, distribution, and reproduction in any medium, provided the original work is properly cited.

How to cite this article: Barzegar H, Chruściel PT and Steininger E. **On elastic deformations of cylindrical bodies under the influence of the gravitational field [version 2; peer review: 3 approved, 1 approved with reservations]** Open Research Europe 2024, **4**:98 https://doi.org/10.12688/openreseurope.17329.2

First published: 10 May 2024, **4**:98 https://doi.org/10.12688/openreseurope.17329.1

REVISED **Amendments from Version 1**

We thank the reviewers for their valuable input. Numerous changes and additions throughout the text were made as suggested to improve the overall work. The main results and applicability of the work were further highlighted and general comprehensibility was enhanced. We especially focused on introducing the experimental setup under consideration and the various models we used in more detail, as well as making clear the logical steps from one section to the next.

Further, additional comparisons of the boundary conditions we employed as approximations to the Hertz contact model were added, quantifying their range of validity. In particular we show that for the main physical observable of interest, namely the total change in length, the precise formulation of the contact model gives only small corrections.

Lastly, we expanded the section on numerical estimates for the GRAVITES experiment to include further discussion on the expected environmental stability and uncertainty estimates.

Any further responses from the reviewers can be found at the end of the article

1 Introduction

An experiment is currently being built [1] with the aim to measure the effect of the gravitational field on entangled states of photons propagating in an optical fiber. The experiment requires displacing vertically an optical fiber, with circular cross-sections, in a spooled configuration. See Figure 1.1 and Figure 1.3 for the configuration of the interferometer after an arm has been moved to a higher position. Such a displacement in the gravitational field of the Earth leads to a minute phaseshift, which is expected to be measurable with the current state-of-the art photonic technology. The displacement is associated with a change of the ambient gravitational acceleration, of temperature, and of atmospheric pressure, leading to an elastic deformation of the fiber. The deformation affects the shape, the length, and the propagation properties of light in the fiber, leading to an additional phaseshift which needs to be determined for a correct interpretation of the results of the experiment.

The objective of this work is to develop a framework which can be used to determine this elastic deformation. This requires in principle a general relativistic theory of elasticity [2–6]. However, it has been shown in [7] that, not unexpectedly, Newtonian elasticity provides a good approximation in the regime we are interested in. The resulting effects on the propagation properties of light in the fiber will be determined elsewhere [8].

The planned configuration is that of a spool with its axis of symmetry aligned vertically. Since the radius of the spool is very large compared to the radius of the fiber, we ignore the spooling and consider a very long elastic cylinder. We then consider several models for the problem at hand:

As a first model we start with a cylindrical waveguide resting on a horizontal contact line (see Figure 1.3a and Section 4.1.1). The next model is a configuration where the waveguide is squeezed between two contact lines, to take into account the pressure arising from the layers pressing from above (see Figure 1.3b and Section 4.1.2).

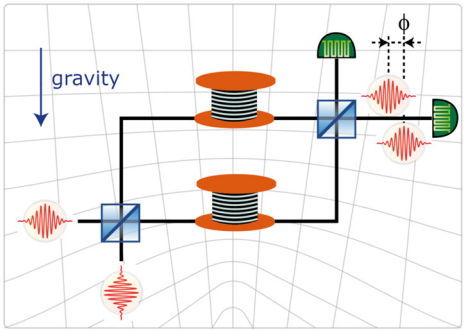


Figure 1.1. The GRAVITES experiment. The upper arm of the interferometer is moved vertically in the height-dependent gravitational field of Earth, indicated by a curving background. The change of the gravitational field due to the change of height affects the propagation of light, resulting in a height-dependent phase shift φ. Both here and in our calculations the y-axis is aligned vertically, so that the gravitational force, indicated by the down-pointing arrow, acts anti-colinearly along the y-axis. In the experimental configuration the axis of the spool is vertical, in order to minimize the deformations of the spool. The radius of the waveguide is much smaller than the radius of the spool, and the slope of the waveguide arising from the spooling is small. This leads us to an approximation where the waveguide is "unwound" to be straight and horizontal. In our calculations the z-direction is aligned with the axis of the unwound waveguide and is horizontal. See also Figure 1.2. © C. Hilweg, reproduced with kind permission of the author.

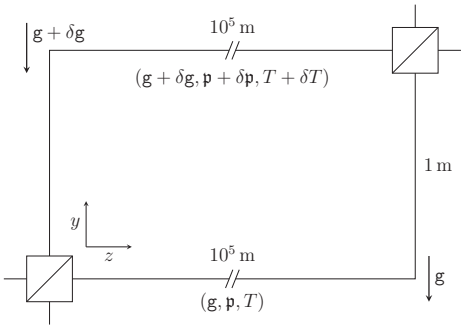


Figure 1.2. Our model for analysing the elastic deformations in GRAVITES. The spools have been unwound so that the center of the waveguide lies on the axis x=y=0. Hence we ignore the curving of the spool and the changes of physical parameters as we move along each individual arm. The coordinate y runs along the vertical. The coordinate z runs along the waveguide.

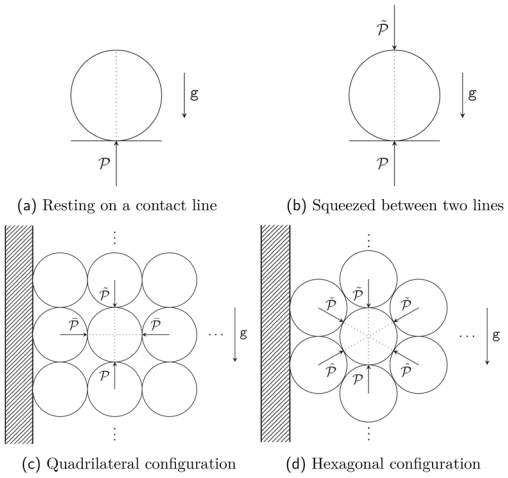


Figure 1.3. The four main models. The y-axis is again along the vertical in all four figures. Figures (**a**) and (**b**) show the cross-section of an infinite cylinder resting on a rigid support, with a supplementary pressure from the top in Figure (**b**). Figures (**c**) and (**d**) show the spool of Figure 1.1 as cut by a vertical plane; we assume that the radius of the spool is very large compared to the radius of the waveguide. The circles represent the consecutive returns of the waveguide, exercising pressure on the neighboring strands. The dashed region represents the rigid spool.

The results obtained in both cases are unacceptable, with an infinite deformation at each contact line; this is of course a well known problem of such models (cf. [9, Chapter 8.4.7]). However, the model appears useful for its simplicity, we will return to this shortly.

To avoid the above problems we pass to a Hertz-contact-type calculation, where we first analyse a configuration with the waveguide resting on a rigid support, followed by one where the waveguides are stacked upon each other; in the last case the influence of the upper layer on a lower one is modelled by contact with a rigid plane. There arises a parameter describing the pressure from the waveguides stacked above the section of the fiber under consideration. We leave this parameter free in our calculations, its value can be determined by the number of layers and windings of the spool whenever a specific configuration is considered.

The above takes into account the vertical neighbours of any given section of the fiber, but ignores the side neighbours. To address this we consider two further configurations, where each fiber has four neighbours as in Figure 1.3c (see Section 4.2.4), or each fiber has six neighbours as in Figure 1.3d and Section 4.2.5. The last model seems to us to provide the best approximation to the problem at hand. In such models new parameters arise, associated with presence of new neighbours. We leave these parameters free again, and show in Appendix A how one of these parameters can be determined for each layer in the quadrilateral-contact case.

Our results show that in all models the relative deformations are similar, for the practical purposes of our interest, close enough to the center of waveguide, where the guiding core resides. Therefore we expect that the first, simplest model, will be sufficient for the applications we have in mind. We address this

question in a future full treatment of the influence of small elastic deformations on the dispersion relation in optical fibers [8].

We include a constant ambient pressure term, as well as temperature effects in all configurations, in order to model possible variations of the environment.

2 Waveguide deformation in Earth's gravity

The unperturbed waveguide is modelled as a very long, homogeneous cylinder with radius a, length L and density ρ, supported by a rigid plane with gravity acting as a body force via a constant gravitational acceleration g. We take $U = \{(r, \theta, z) : 0 < r \leq a, -\pi < \theta \leq \pi, 0 \leq z \leq L\}$ to be the interior of the waveguide and write ∂U for the surface $r = a$. Note that $a \ll L$. We will consider the four configurations depicted in Figure 2.1 (a)–(d). The elastic deformations that are of interest to us are minute, therefore we will apply the linear theory of elastic deformations, including thermoelasticity. Such deformations are described by a field u_i which describes the (small) displacements of a body part from a position which arises when no forces are applied on the system. One then defines the associated *strain tensor*:

$$\epsilon_{ij} = \frac{1}{2}(\partial_i u_j + \partial_j u_i)\,. \tag{2.1}$$

This induces stresses in the material, described by the *stress tensor* σ_{ij}. Assuming isotropy, the generalized Hooke law in three dimensions takes the form of the following stress-strain relation (cf., e.g., [9, Eq. (4.2.7)] and [10, Eq. (4.6)]),

$$\sigma_{ij} = \lambda \epsilon_{kk}\, \delta_{ij} + 2\mu \epsilon_{ij}, \tag{2.2}$$

Here λ and μ are respectively Lamé's first and second parameters of the material. The parameter μ, called the shear modulus, is sometimes denoted by G in the literature. We only consider homogeneous materials, where the Lamé parameters are taken to be constant throughout the material. Repeated indices are summed over unless explicitly indicated otherwise. Here, and elsewhere, all tensors are expressed in orthonormal frames. With $\sigma_{kk} = (3\lambda + 2\mu)\epsilon_{kk}$ we find

$$\epsilon_{ij} = \frac{1+\nu}{E}\sigma_{ij} - \frac{\nu}{E}\sigma_{kk}\,\delta_{ij}, \tag{2.3}$$

where $E := \mu(3\lambda + 2\mu)/(\lambda + \mu)$ is Young's modulus and $\nu := \lambda/[2(\lambda + \mu)]$ is Poisson's ratio. Note that $E = 2\mu(1 + \nu)$.

When the changes of temperature are *not* negligible, the above needs to be revised as follows: According to [9, Section 4.4], in a thermally-isotropic and thermally-linear medium, Equation (2.3) should be replaced by

$$\epsilon_{ij} = \frac{1+\nu}{E}\sigma_{ij} - \frac{\nu}{E}\sigma_{kk}\,\delta_{ij} + \alpha(T - T_0)\,\delta_{ij}, \tag{2.4}$$

where α is the *coefficient of linear thermal expansion*, which we assume to be constant throughout the material. This is a consequence of the assumptions of linear thermo-elasticity, for which the strain decomposes into independent thermal and elastic components. Inverting this relation, the stress tensor is given by

$$\sigma_{ij} = \lambda \epsilon_{kk}\,\delta_{ij} + 2\mu\epsilon_{ij} - (3\lambda + 2\mu)\,\alpha(T - T_0)\delta_{ij}. \tag{2.5}$$

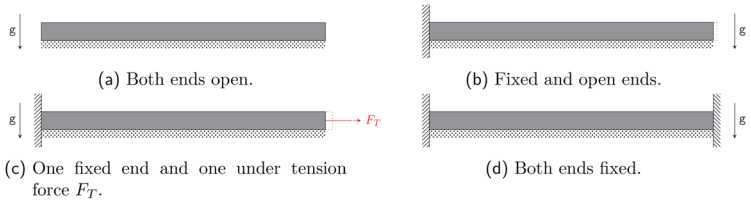


Figure 2.1. Four models for a very long cylinder with boundary conditions covered by our calculations. Vertical dashed regions represent fixed ends in the z-direction, whereas the dotted bars represent rigid supports. The remaining boundaries in the figures can move freely. The presence of a tension force F_T in Figure (**c**) is relevant for the boundary conditions in the z-direction and its effect will be analysed in Section 3. Note that the model (**d**) requires the vanishing of the elongation coefficient κ of (2.6).

We allow the waveguide to stretch in the z direction linearly in z,

$$u_z = \kappa z. \tag{2.6}$$

All remaining fields are assumed to be z-independent. While we will consider all four configurations in Figure 2.1, the one that we are most interested in is configuration (**c**). In that case we have displacement-free boundary conditions on one end while needing to match the stress at the other end to the externally imposed force F_T. We assume that F_T remains constant when moving the spools in the gravitational field, and its precise value drops out when calculating the changes of the deformations (cf. Equation (3.17) below).

Equation (2.6) leads to a non-vanishing z-component of the strain tensor, namely

$$\epsilon_{zz} = \kappa, \quad \text{but} \quad \epsilon_{xz} = \epsilon_{yz} = 0, \tag{2.7}$$

giving an additional contribution to the usual plane-strain relations (cf. [11] for related considerations).

Having reduced the dimensionality of the problem, the equilibrium equations (cf., e.g., [9, Eq. (3.6.4)] or [12, Eq. (2.34)]),

$$\partial_j \sigma_{ij} + F_i = 0, \tag{2.8}$$

with σ_{ij} the stress tensor and $F_i = -\partial_i V$ the body force due to gravity, where $V = g\rho y$, simplify to

$$\partial_x \sigma_{xx} + \partial_y \sigma_{xy} - \partial_x V = 0, \tag{2.9}$$

$$\partial_x \sigma_{xy} + \partial_y \sigma_{yy} - \partial_y V = 0. \tag{2.10}$$

where we used Cartesian coordinates (x,y,z), in which the Euclidean metric equals $dx^2 + dy^2 + dz^2$. Note that the stress in the z-direction does not necessarily vanish. Indeed, the zz-component of (2.4) gives

$$\kappa = \frac{\sigma_{zz}}{E} - \frac{\nu}{E}(\sigma_{xx} + \sigma_{yy}) + \alpha(T - T_0), \tag{2.11}$$

so that all the elasticity equations, including Equation (2.8) will be satisfied by setting $\sigma_{zx} = \sigma_{zy} = 0$ and

$$\sigma_{zz} = \nu(\sigma_{xx} + \sigma_{yy}) + E\kappa - E\alpha(T - T_0). \tag{2.12}$$

We wish to solve Equation (2.9)–Equation (2.10) for gravitating systems which include the GRAVITES experiment. For this we will use the fact that solutions of these equations can be parameterised by the *Airy stress function* ϕ (cf. [13] and, e.g., [14, Eqs. (8.12)–(8.13)]) as

$$\sigma_{ij} = \left(\Delta_\delta \phi + V\right)\delta_{ij} - D_i D_j, \tag{2.13}$$

where D_i denotes the covariant derivative of the Euclidean metric $dx^2 + dy^2 = dr^2 + r^2 d\theta^2$ on $\mathbb{R}^2$, and Δ_δ its Laplacian (the formula with $V = 0$ parameterises thus all divergence-free symmetric tensors).

Adapting our coordinate system to the symmetry of the setup by choosing cylindrical coordinates, from now on tensor components will refer to the following orthonormal frame, which in Cartesian coordinates is given by

$$e_r := (\cos(\theta), \sin(\theta), 0), \quad e_\theta := (-\sin(\theta), \cos(\theta), 0), \quad e_z := (0,0,1). \tag{2.14}$$

In this frame the stress tensor can be expressed in terms of derivatives of the Airy stress function ϕ and of the gravitational potential V as

$$\sigma_{rr} = \frac{1}{r}\partial_r \phi + \frac{1}{r^2}\partial_\theta^2 \phi + V, \tag{2.15}$$

$$\sigma_{\theta\theta} = \partial_r^2 \phi + V, \tag{2.16}$$

$$\sigma_{r\theta} = -\partial_r\left(\frac{1}{r}\partial_\theta \phi\right), \tag{2.17}$$

The Airy function has to satisfy the "compatibility condition" (see, e.g., [6, Proposition 4.31], [9, Eq. (7.5.5)] or [12, Eq. (7.17b)], together with [9, Eq. (12.3.7)]),

$$\Delta_\delta^2 \phi = -\frac{1-2\nu}{1-\nu}\Delta_\delta V - \frac{E\alpha}{1-\nu}\Delta_\delta T, \tag{2.18}$$

(Note that V is only defined up to a constant, which can be absorbed by a redefinition of ϕ.) In this work we consider a steady-state configuration, which requires $\Delta_\delta T = 0$ (cf. [9, Section 12.1]). Further, since $V = g\rho y$ we have $\Delta_\delta V = 0$ as well, implying that the compatibility conditions reduce to the homogeneous biharmonic equation.

Since the frame $\{e_r, e_\theta, e_z\}$ is orthonormal, the strain is related to the stress via (2.4):

$$\epsilon_{rr} = \frac{1}{2\mu}[(1-\nu)\sigma_{rr} - \nu\sigma_{\theta\theta}] - \nu\kappa + (1+\nu)\alpha(T - T_0), \tag{2.19}$$

$$\epsilon_{\theta\theta} = \frac{1}{2\mu}[(1-\nu)\sigma_{\theta\theta} - \nu\sigma_{rr}] - \nu\kappa + (1+\nu)\alpha(T - T_0), \tag{2.20}$$

$$\epsilon_{r\theta} = \frac{1}{2\mu}\sigma_{r\theta}. \tag{2.21}$$

One can now determine the displacement vector u_i from the usual equations, where u_r and u_θ are frame components of u (cf., e.g., [9, Eq. (7.6.1)])

$$\epsilon_{rr} = \partial_r u_r, \tag{2.22}$$

$$\epsilon_{\theta\theta} = \frac{1}{r}(\partial_\theta u_\theta + u_r), \tag{2.23}$$

$$\epsilon_{r\theta} = \frac{1}{2}\left(\frac{1}{r}\partial_\theta u_r + \partial_r u_\theta - \frac{1}{r}u_\theta\right). \tag{2.24}$$

Having compiled all relevant equations from linear elasticity, we set up an adapted coordinate system as in Figure 2.2, with

$$r \in (0, a] \text{ and } \theta \in (-\pi, \pi]. \tag{2.25}$$

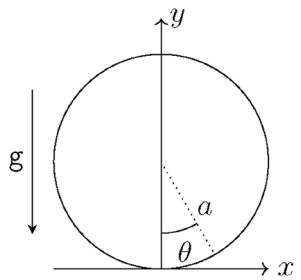


Figure 2.2. Convention for polar coordinates.

There exists a general solution for (2.18) in polar coordinates, denoted by[1]

$$\begin{aligned}\phi(r,\theta) = {} & A_0 \ln r + B_0 + C_0 r^2 \ln r + D_0 r^2 \\ & + \left(a_0 \ln r + b_0 + c_0 r^2 \ln r + d_0 r^2\right)\theta \\ & + \left(A_1 r \ln r + \frac{B_1}{r} + C_1 r^3 + D_1 r + E_1 r\theta + F_1 r\theta \ln r\right)\cos(\theta) \\ & + \left(a_1 r \ln r + \frac{b_1}{r} + c_1 r^3 + d_1 r + e_1 r\theta + f_1 r\theta \ln r\right)\sin(\theta) \\ & + \sum_{n\geq 2}\Big[\left(A_n r^n + B_n r^{-n} + C_n r^{n+2} + D_n r^{2-n}\right)\cos(n\theta) \\ & \qquad + \left(a_n r^n + b_n r^{-n} + c_n r^{n+2} + d_n r^{2-n}\right)\sin(n\theta)\Big],\end{aligned} \tag{2.26}$$

known as the 'Michell solution' [15].

In practical terms, we are mostly concerned with determining the coefficients in (2.26) from the boundary conditions we impose. An immediate simplification can be achieved by only considering solutions which have the mirror symmetry $x \mapsto -x$ (equivalently $\theta \mapsto -\theta$), since the forces considered are invariant under this symmetry; see Appendix B for a treatment without imposing mirror symmetry at the outset. Additionally, we require regularity at $r = 0$ and 2π-periodicity in θ. Restricting to mirror-symmetric boundary conditions finally leads to a requirement of mirror-symmetry in σ_{rr} and $\sigma_{\theta\theta}$ and antisymmetry for $\sigma_{r\theta}$. Lastly, note that the parameters B_0 and D_1 do not contribute to the stress as by Equation (2.15)–Equation (2.17), which is straightforwardly verified. They may be considered degeneracies of the solution space and set to zero without loss of generality (cf. [14]). The remaining terms in (2.26) are

$$\phi(r,\theta) = D_0 r^2 + C_1 r^3 \cos(\theta) + \sum_{n\geq 2}\left(A_n r^n + C_n r^{n+2}\right)\cos(n\theta), \tag{2.27}$$

which is the form considered for all applications below.

The displacement can be calculated via (2.22)–(2.24)[2]. We have for the remaining terms in ϕ,

$$\begin{aligned}u_r(r,\theta) = {} & \frac{1}{2\mu}\Bigg\{2(1-2\nu)D_0 r + (1-4\nu)C_1 r^2\cos(\theta) - \frac{1}{2}g\rho(1-2\nu)r^2\cos(\theta) \\ & + \sum_{n\geq 2}\left[-nA_n r^{n-1} + (2-4\nu-n)C_n r^{n+1}\right]\cos(n\theta)\Bigg\} - \Xi\cos(\theta) - \nu k r \\ & + (1+\nu)\alpha(T-T_0)r,\end{aligned} \tag{2.28}$$

$$\begin{aligned}u_\theta(r,\theta) = {} & \frac{1}{2\mu}\Bigg\{(5-4\nu)C_1 r^2\sin(\theta) - \frac{1}{2}g\rho(1-2\nu)r^2\sin(\theta) \\ & + \sum_{n\geq 2}\left[nA_n r^{n-1} + (4-4\nu+n)C_n r^{n+1}\right]\sin(n\theta)\Bigg\} + \Xi\sin(\theta) + c^* r,\end{aligned} \tag{2.29}$$

where c^*, Ξ are integration constants. These are fixed by the boundary conditions imposed at the contact point $u_r(a, 0) = 0 = u_\theta(a, 0)$, which imply $c^* = 0$ and

$$\begin{aligned}\Xi := \frac{1}{2\mu}\Bigg\{ & 2(1-2\nu)D_0 a + (1-4\nu)C_1 a^2 - \frac{1}{2}g\rho(1-2\nu)a^2 \\ & + \sum_{n\geq 2}\left[-nA_n a^{n-1} + (2-4\nu-n)C_n a^{n+1}\right]\Bigg\} - \nu\kappa a + (1+\nu)\alpha(T-T_0)a,\end{aligned} \tag{2.30}$$

provided that the sums converge.

[1] The redefinition $\theta \to \theta - \frac{\pi}{2}$ can be absorbed by the constants.

[2] A convenient form for the full parametrized solution can be found in [14, Tab. (9.1)].

3 Boundary conditions

We now have general expressions for the stresses (2.15)–(2.17), the strains (2.19)–(2.21), and the displacements (2.28)–(2.29), in terms of the coefficients $\{D_0, C_1, A_n, C_n\}$ for $n \geq 2$. These coefficients can be determined from the boundary conditions algebraically.

To proceed further one needs to specify the boundary conditions satisfied by the bodies of interest. At the boundary of the cylinder we consider an angle dependent pressure $f(\theta)$ acting in the radial direction and a shear force per unit area $g(\theta)$. The boundary conditions in linear elasticity require the stresses at the boundary to react to the external forces as

$$\sigma_{r\theta}|_{\partial U} = g(\theta), \tag{3.1}$$

$$\sigma_{rr}|_{\partial U} = f(\theta). \tag{3.2}$$

Our assumption of mirror-symmetry implies that the boundary conditions can be Fourier decomposed into sine and cosine series respectively,

$$\sigma_{r\theta}|_{\partial U} = \sum_{n\geq 0} g_n \sin(n\theta), \tag{3.3}$$

$$\sigma_{rr}|_{\partial U} = \frac{1}{2} f_0 + \sum_{n\geq 1} f_n \cos(n\theta), \tag{3.4}$$

with the coefficients given explicitly by

$$g_n = \frac{2}{\pi}\int_0^\pi \mathrm{d}\theta\, g(\theta)\sin(n\theta), \tag{3.5}$$

$$f_n = \frac{2}{\pi}\int_0^\pi \mathrm{d}\theta\, f(\theta)\cos(n\theta). \tag{3.6}$$

On the other hand, we know that the solution can be written using (2.15)–(2.17) with (2.27) for the Airy stress function; explicitly

$$\sigma_{r\theta}|_{\partial U} = 2C_1 a\sin(\theta) + \sum_{n\geq 2}\Big[(n-1)A_n + a^2(n+1)C_n\Big] n a^{n-2}\sin(n\theta), \tag{3.7}$$

$$\sigma_{rr}|_{\partial U} = 2D_0 + (2C_1 - \mathrm{g}\rho)\, a\cos(\theta) - \sum_{n\geq 2}\Big[(n-1)nA_n + a^2(n^2-n-2)C_n\Big] a^{n-2}\cos(n\theta). \tag{3.8}$$

Comparing term by term determines the coefficients. We are generally interested in the case with vanishing shear forces, i.e. $g(\theta) = 0$, which corresponds to only normal forces or the frictionless limit. Then,

$$C_1 = 0 \text{ and } C_n = \frac{1-n}{a^2(1+n)} A_n, \tag{3.9}$$

and for the radial stress

$$\sigma_{rr}|_{\partial U} = 2D_0 - a\mathrm{g}\rho\cos(\theta) - 2\sum_{n\geq 2} A_n (n-1) a^{n-2}\cos(n\theta). \tag{3.10}$$

Comparing coefficients with (3.4), we find

$$D_0 = \frac{1}{4} f_0, \tag{3.11}$$

$$A_n = -\frac{1}{2(n-1)} a^{2-n} f_n, \tag{3.12}$$

for $n \geq 2$, with

$$f_1 = -a\mathrm{g}\rho. \tag{3.13}$$

We see that the Fourier coefficient f_1 in the function f in (3.2) is not arbitrary, and is determined by the body force.

The boundary conditions in the z-direction are given by the models shown in Figure 2.1. We focus on subfigure (c), with the special case without tension force F_T corresponding to subfigure (b). By definition, the displacement boundary conditions are given by (2.6), since we allow for elongation of the open end. The boundary condition for the stress is given by

$$F_T = \int_{U(z=L)} \sigma_{zz}\, r\, \mathrm{d}r\, \mathrm{d}\theta, \tag{3.14}$$

i.e. the forces on the end face of the cylinder have to match the stresses on the end face. Using (2.12), this can be rewritten as

$$F_T = \int_{U(z=L)} \nu(\sigma_{xx}+\sigma_{yy}) r\, \mathrm{d}r\, \mathrm{d}\theta + \pi a^2 E[\kappa - \alpha(T-T_0)]. \tag{3.15}$$

The integral can be calculated either explicitly or numerically for the solutions in Section 4, providing thus a relation between the forces acting on the system, κ, and the remaining parameters that appear in the problem.

This can be restated as an equation for the elongation coefficient κ as a function of tension F_T and the plane stresses along the fiber:

$$\kappa = -\frac{1}{\pi a^2 E}\int_{U(z=L)} \nu(\sigma_{xx}+\sigma_{yy}) r\, \mathrm{d}r\, \mathrm{d}\theta + \alpha(T-T_0) + \frac{F_T}{\pi a^2 E}. \tag{3.16}$$

For a waveguide of total length L, this implies a change in length

$$L \mapsto L + \kappa L = L\left[1 - \frac{1}{\pi a^2 E}\int_{U(z=L)} \nu(\sigma_{xx}+\sigma_{yy}) r\, \mathrm{d}r\, \mathrm{d}\theta + \alpha(T-T_0) + \frac{F_T}{\pi a^2 E}\right]. \tag{3.17}$$

Note that the length can change even if F_T vanishes.

Given a spooling force and upon specifying ambient gravity, pressure, and temperature, Equation (3.17) allows the computation of the length of each arm of the interferometer. Now, due to the arms' one-meter vertical spacing, the ambient variables will be different for each arm. We should therefore expect each arm of the interferometer to be of different length. This difference in length will lead to an extra phase-shift that must be taken into account and that is derived directly from Equation (3.17). In Section 4 we proceed to derive expressions for σ_{xx} and σ_{yy} in terms of ambient pressure, temperature, and gravity, so that the differences $\delta\mathfrak{p}$, δT, and $\delta\mathrm{g}$ of $\mathfrak{p}$, T and g indeed provide, via Equation (3.17), a formula for the change of the length of an arm after displacement.

Equation (3.17) is one of key results in this work, as it will allow us to determine the associated change of phase of photons exiting the waveguide. We expect this to be the dominant effect of elasticity on the phase in a perfectly isolated system. This expectation is confirmed in follow-up work [8], where the influence of all elastic deformations derived in this work on Maxwell fields is determined.

4 Contact models

Having formally solved the problem for arbitrary boundary conditions in the preceding section, we now implement the boundary conditions for the configurations shown in Figures 1.3a–1.3d.

As already pointed out in the Introduction, the solutions for the configurations of Figures 1.3a–1.3b, that we are about to derive, with the boundary conditions corresponding to contact lines, describe unphysical displacement fields, diverging at the contact interfaces. We show that this can be cured by deriving a solution involving extended contact regions, using the Hertz contact deformations formalism. We show that even though the displacements differ between these approaches, the stresses near the center of the waveguide are in reasonable agreement.

4.1 Line contacts

4.1.1 Resting on a contact line. We start with the analysis of the simplest physical model, given by a cylindrical waveguide lying on an infinite plane, contacting (as a first approximation) only on a line. This is reminiscent of the famous Flamant solution with circular cross-section (see in particular [14, Problem 3 of Chapter 12]).

The boundary conditions are given by

$$\sigma_{r\theta}|_{\partial U} = 0, \tag{4.1}$$

$$\sigma_{rr}|_{\partial U} = -\mathcal{P}\delta(\theta) - \mathfrak{p}, \tag{4.2}$$

where $\mathcal{P}$ is the pressure with which the contact line is resisting the weight of the waveguide and $\mathfrak{p}$ the ambient pressure, taken to be constant. To put this into physical terms, we apply neither tangential nor radial forces, except for the contact line with the "contact wire".

This model is particularly convenient, since the δ-distribution has a Fourier series expansion as

$$\delta(\theta) = \frac{1}{2\pi}\left[1 + 2\sum_{1\le n}\cos(n\theta)\right]. \tag{4.3}$$

We find for the coefficients in the Michell solution

$$D_0 = -\frac{\mathcal{P}}{4\pi} - \frac{\mathfrak{p}}{2}, \tag{4.4}$$

$$C_1 = 0, \tag{4.5}$$

$$A_n = \frac{\mathcal{P}}{2\pi a^{n-2}(n-1)}, \tag{4.6}$$

$$C_n = -\frac{\mathcal{P}}{2\pi a^{n}(n+1)}, \tag{4.7}$$

with

$$\mathcal{P} = \pi a \mathrm{g}\rho, \tag{4.8}$$

as follows from the condition Equation (3.13).

This last constraint implements the physicality of the calculations, since in the absence of other forces there can only be an equilibrium configuration if the integrated body force of the waveguide

$$\int(-F_y) r\,\mathrm{d}r\mathrm{d}\theta = \int \mathrm{g}\rho\, r\,\mathrm{d}r\mathrm{d}\theta = \pi a^2 \mathrm{g}\rho, \tag{4.9}$$

matches the reactive force exerted by the plane, given by

$$\int \mathcal{P}\delta(\theta) r\,\mathrm{d}\theta|_{\partial U} = \pi a^2 \mathrm{g}\rho. \tag{4.10}$$

The sum in (2.27) converges for coefficients (4.4)–(4.7), yielding

$$\phi(r,\theta) = -\frac{1}{2}r^2\mathfrak{p} + \frac{1}{4}r\mathrm{g}\rho\left[r\,(a + r\cos(\theta)) - 4a^2\arctan\left(\frac{r\sin(\theta)}{a - r\cos(\theta)}\right)\sin(\theta)\right], \tag{4.11}$$

and further for the stresses

$$\sigma_{rr} = A\Big[r\,(6a^2 + r^2)\cos(\theta) - a\Big(a^2 + 3r^2 + 2(a^2 + r^2)\cos(2\theta) - ar\cos(3\theta)\Big)\Big] - \mathfrak{p}, \tag{4.12}$$

$$\sigma_{r\theta} = A\Big[4a(a^2+r^2)\cos(\theta) - r\left(5a^2+r^2+2a^2\cos(2\theta)\right)\Big]\sin(\theta), \tag{4.13}$$

$$\sigma_{\theta\theta} = A\Big[-r(2a^2+r^2)\cos(\theta) + a\left(r^2-a^2+2(a^2+r^2)\cos(2\theta) - ar\cos(3\theta)\right)\Big] - \mathfrak{p}, \tag{4.14}$$

with

$$A := \frac{\mathrm{g}\rho(a^2-r^2)}{2[a^2+r^2-2ar\cos(\theta)]^2}.$$

A representative plot of the stresses can be seen in Figure 4.1.

Equation (2.28)–Equation (2.30) do not make sense, as the sum in Ξ does not converge. But one can find explicit expressions for u_r and u_θ by integration; the resulting formulae are lengthy and not very enlightening, therefore we did not include them here. Not unexpectedly, and similar to the Flamant solution [9, Chapter 8.4.7] , the singularity in the function A at $r = a$ and $\cos\theta = 1$ leads to an infinite displacement there. Hence the boundary condition $u(r = a,\ \theta = 0) = 0$ cannot be imposed. However, the displacements obtained by direct integration are finite

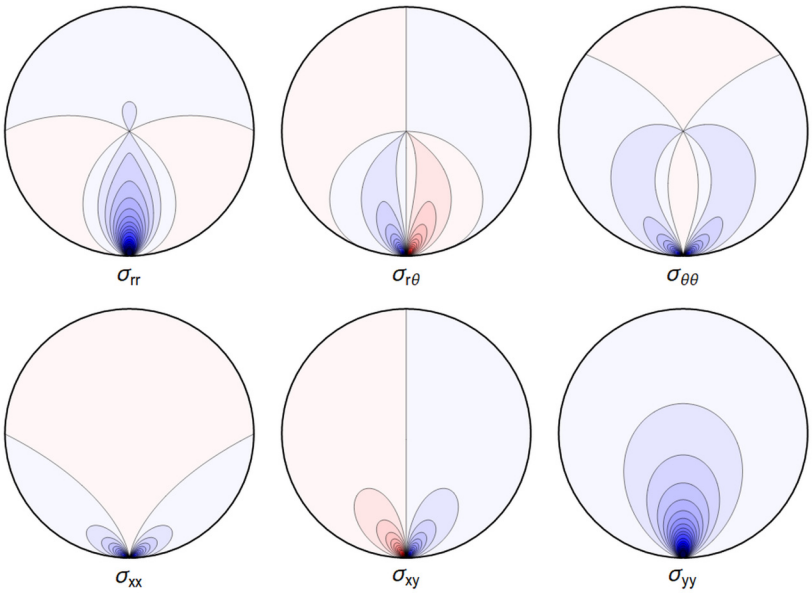


Figure 4.1. Typical plot of internal stresses for the case of a waveguide resting on an infinitely thin line, with unrealistic parameters arbitrarily chosen for illustration purposes listed in Table 4.1. Here, and in all similar figures, shades of blue indicate compressive (negative) stresses, shades of red indicate positive ones, with darker colors encoding larger stresses.

Table 4.1. Set of parameters chosen in our visualizations. For conciseness, we express lengths in multiples of a, and pressure in multiples of the shear modulus μ, leading to dimensionless quantities for the remaining parameters used in numerical calculations.

$\rho\mathrm{g}$	ν	$\mathfrak{p}$, κ, α	$\tilde{\mathcal{P}}$	$\hat{\mathcal{P}} = \check{\mathcal{P}}$
0.01	0.17	0	1	0.3

away from the contact point, in particular near the center of the waveguide (cf. [16]). One can also truncate the series (2.28)–(2.29) which leads to finite solutions, illustrated in Figure 4.2.

4.1.2 Squeezed between two lines. In a waveguide wound on a spool, consecutive layers of the waveguide press onto each other. The simplest model for this is a cylinder squeezed between two contact lines, with a pressure $\tilde{\mathcal{P}}$ pushing from the top, as in Figure 1.3b. See also [9, Example 8–10] and [14, Problem 1 of Chapter 12], where a similar problem is modelled by superposition of three particular stress fields, including two Flamant solutions together with a uniform radial tension loading. The boundary conditions are given by

$$\sigma_{r\theta}|_{\partial U} = 0, \tag{4.15}$$

$$\sigma_{rr}|_{\partial U} = -\mathcal{P}\delta(\theta) - \tilde{\mathcal{P}}\delta(\theta-\pi) - \mathfrak{p}. \tag{4.16}$$

The calculation is completely analogous to the above, with the boundary condition enforcing

$$D_0 = -\frac{\mathcal{P}+\tilde{\mathcal{P}}}{4\pi} - \frac{\mathfrak{p}}{2}, \tag{4.17}$$

$$C_1 = 0, \tag{4.18}$$

$$A_n = \frac{\mathcal{P}+(-1)^n\tilde{\mathcal{P}}}{2\pi a^{n-2}(n-1)}, \tag{4.19}$$

$$C_n = -\frac{\mathcal{P}+(-1)^n\tilde{\mathcal{P}}}{2\pi a^{n}(n+1)}, \tag{4.20}$$

with the force-balancing condition Equation (3.13) now reading

$$\mathcal{P} = \tilde{\mathcal{P}} + \pi a g \rho. \tag{4.21}$$

Again, the physical interpretation is that now the force from above necessitates a reactive force from below larger than in (4.8) to achieve equilibrium.

Denoting by σ^I_{ij} the right-hand sides of (4.12)–(4.14), the stress components read

$$\sigma_{rr} = \sigma^I_{rr} - B\,(a^2-r^2)\left[a^4 - 2a^2r^2 - r^4 + 2a^4\cos(2\theta)\right], \tag{4.22}$$

$$\sigma_{r\theta} = \sigma^I_{r\theta} + 2Ba^2(a^4-r^4)\sin(2\theta), \tag{4.23}$$

$$\sigma_{\theta\theta} = \sigma^I_{\theta\theta} - B\left[a^6 + 5a^4r^2 + a^2r^4 + r^6 - 2a^2(a^4+a^2r^2+2r^4)\cos(2\theta)\right], \tag{4.24}$$

with $B := -\frac{\tilde{\mathcal{P}}}{\pi}(a^2-r^2)\,[a^4+r^4-2a^2r^2\cos(2\theta)]^{-2}$. Again, visualizing the result gives a clear picture. See Figure 4.3.

As before, the deformation diverges at the "contact wires". A truncated sum is shown in Figure 4.4.

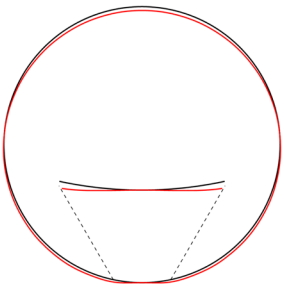


Figure 4.2. Illustrative deformation for the case of a waveguide resting on an infinitely thin line, after truncating the sums in (2.28)–(2.30) to n = 20, drawn in red. The undeformed reference is drawn in black. Here and in similar figures below, the inset shows a magnified section around the contact point.

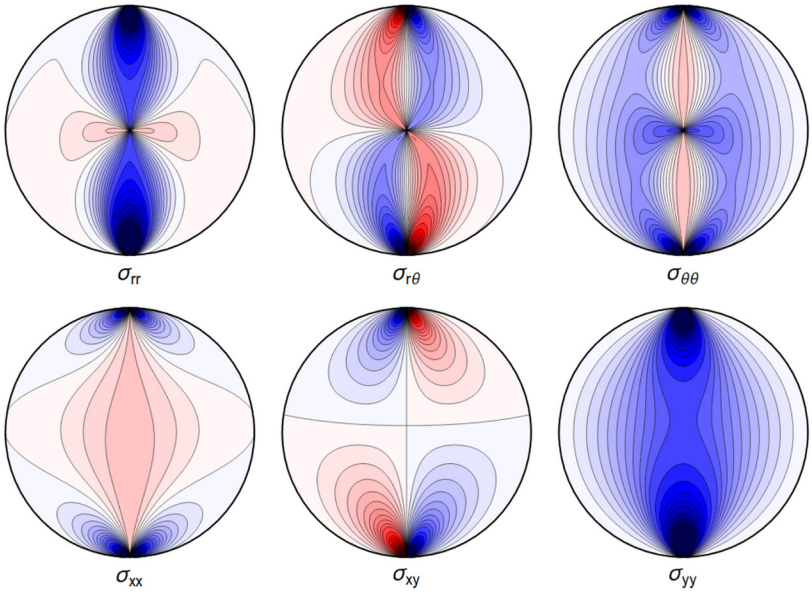


Figure 4.3. Typical plot of internal stresses for the case of a waveguide squeezed between two lines; same parameters and color coding as in Figure 4.1.

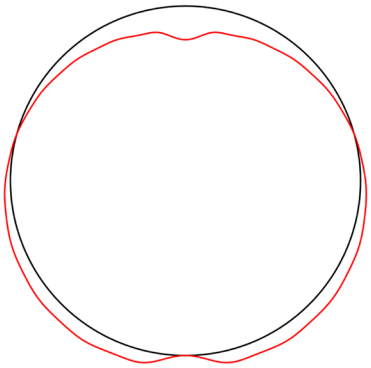


Figure 4.4. Illustrative deformation for the case of a waveguide squeezed between two lines, after truncating the sums in (2.28)–(2.30) to $n = 20$, drawn in red. The undeformed reference is drawn in black.

4.2 Hertz contact deformations

In view of the above divergences, a better model for the contact between the waveguide and its support, or between neighbouring strands of the waveguide, is needed. A possible solution for this in linear elasticity is given by the Hertz contact deformation [17], with a modern derivation given by [10, Chapter 9].

To implement this we consider two cylinders contacting lengthwise. The contact region, which was previously described as a line, becomes a strip. On each cross-section, the contact point of the previous analysis becomes an interval (cf. [10, Problem 2 of Chapter 9]). The total force $\mathbb{F}$ per unit length pushing two bodies into each other is now distributed over a region $\{x : -s \le x \le s\}$, where

$$s = \sqrt{\frac{4\mathbb{F}}{\pi}\left(\frac{1-\nu^2}{E} + \frac{1-\nu'^2}{E'}\right)\frac{RR'}{R+R'}}, \tag{4.25}$$

with $\{\nu,\ E,\ R\}$ the material properties and radius of curvature of the body in question and $\{\nu',\ E',\ R'\}$ for the body in contact. In this model the pressure distribution over the contact region, which we denote by P_y, equals

$$P_y = \frac{2\mathbb{F}}{\pi s}\sqrt{1-\frac{x^2}{s^2}}. \tag{4.26}$$

This can be restated in the form of boundary conditions

$$\sigma_{r\theta}|_{\partial U} = 0, \tag{4.27}$$

$$\sigma_{rr}|_{\partial U} = \begin{cases} \dfrac{2\mathbb{F}}{\pi a \tan(\Theta)}\sqrt{1-\dfrac{\tan^2(\theta)}{\tan^2(\Theta)}} & -\Theta \le \theta \le \Theta \\ 0 & \text{otherwise} \end{cases}, \tag{4.28}$$

where

$$\Theta = \arctan\left(\frac{s}{a}\right). \tag{4.29}$$

For the case of an infinite cylinder resting on a rigid plane, we simply take $R',\ E' \to \infty$ and $\nu' \to 0$.

Finding the cosine expansion of (4.28) is not obvious. Instead, we will approximate the Hertz profile with a step-function as in Figure 4.5, with straightforward cosine expansion, allowing us to find explicit expressions for the Airy functions and stresses in the settings discussed below. The half-width of the step function can be determined, based on the Hertz solution, to

$$s_{\text{Hertz}} = \sqrt{\frac{4a\mathbb{F}}{\pi}\frac{1-\nu^2}{E}}, \tag{4.30}$$

$$\Theta_{\text{Hertz}} = \arctan\left(\frac{s_{\text{Hertz}}}{a}\right), \tag{4.31}$$

via (4.25) and (4.29), ensuring a physically motivated boundary pressure distribution in response to external forces.

For the purpose of the GRAVITES experiment the key role is played by a) the change of length of the waveguide and b) the deformations near the center of the waveguide, where the core of the waveguide is located and where the photons propagate, with the energy of the waves decaying exponentially fast in the cladding. In Figure 4.10 and Figure 4.11 below we show a typical plot of differences between the point-contact solution and our variation of the Hertz-type solution. The figures make it clear that the differences are subdominant in the region of interest. In Figure 4.12 we further show that the difference between the Hertz-type solution and the step-function model is negligible for all our purposes. Our calculations show that both the point-contact approximation and the step-function approximation provide a good approximation for weak forces and away from the contact region, with a numerical comparison provided in Section 4.2.3.

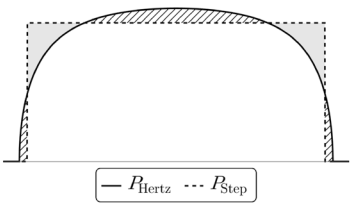


Figure 4.5. Comparison of the pressure distribution in the contact region for the exact Hertz solution (4.28) and an approximation using constant pressure in the contact region. The shaded and dashed regions cause overshoot and undershoot in the displacement figures below.

4.2.1 Resting on a rigid plane. We apply the above to a waveguide resting on a plane, as in Figure 1.3a. Approximating the Hertz contact solution of Section 4.2 by a step-function of constant pressure $\mathcal{P}$ for a single contact region from below leads to the boundary conditions

$$\sigma_{r\theta}|_{\partial U} = 0, \tag{4.32}$$

$$\sigma_{rr}|_{\partial U} = -\mathcal{P}\chi_{[-\Theta,\Theta]}(\theta) - \mathfrak{p}\,(1-\chi_{[-\Theta,\Theta]}(\theta)) =: -\mathcal{P}'\chi_{[-\Theta,\Theta]}(\theta) - \mathfrak{p}, \tag{4.33}$$

with $\Theta := \Theta_{\text{Hertz}}$ as defined in Equation (4.31), where for any set Ω we set

$$\chi_{\Omega}(x) := \begin{cases} 1 & x \in \Omega \\ 0 & \text{else} \end{cases}. \tag{4.34}$$

By assumption our boundary conditions for σ_{rr} are mirror-symmetric with respect to the vertical axis and 2π-periodic. We can write a general formula for the Fourier cosine expansion of their symmetrized sum. For $\Psi,\Theta \in [0,\pi]$ we have,

$$\chi_{[\Psi-\Theta,\Psi+\Theta]}(\theta) + \chi_{[-\Psi-\Theta,-\Psi+\Theta]}(\theta) = \frac{2\Theta}{\pi} + \sum_{n\geq 1} \frac{4\cos(n\Psi)\sin(n\Theta)}{\pi n}\cos(n\theta). \tag{4.35}$$

When $\Psi = 0$ we obtain the following coefficients in (2.27):

$$D_0 = -\frac{\mathcal{P}'\Theta}{2\pi} - \frac{\mathfrak{p}}{2}, \tag{4.36}$$

$$C_1 = 0, \tag{4.37}$$

$$A_n = \frac{\mathcal{P}'\sin(n\Theta)}{\pi a^{n-2} n(n-1)}, \tag{4.38}$$

$$C_n = -\frac{\mathcal{P}'\sin(n\Theta)}{\pi a^{n} n(n+1)}, \tag{4.39}$$

With condition Equation (3.13) reading

$$\mathcal{P}' = \frac{ag\rho\pi}{2\sin(\Theta)}. \tag{4.40}$$

The summed expression for the Airy function is

$$\phi_{\text{single}} = \frac{1}{4}g\rho\left[(2a^2+r^2)r\cos(\theta) - ar^2\frac{\Theta}{\sin(\Theta)} + \frac{a}{\sin(\Theta)}(\zeta(\theta-\Theta) - \zeta(\theta+\Theta))\right] - \frac{1}{2}r^2\mathfrak{p}, \tag{4.41}$$

where the subscript "single" refers to a single contact region, with

$$\zeta(x) := \left[a^2 + r^2 - 2ar\cos(x)\right]\arctan\left(\frac{r\sin(x)}{a - r\cos(x)}\right). \tag{4.42}$$

All the sums converge, leading to an admissible displacement field. The stresses and the displacements are shown in Figure 4.6 and Figure 4.7.

4.2.2 Squeezed between two rigid planes. The next simplest description of a spooled waveguide is one with extended contact regions both above and below. We model this by squeezing the fiber between two rigid planes in the spirit of Section 4.2.1, i.e. boundary conditions

$$\sigma_{r\theta}|_{\partial U} = 0, \tag{4.43}$$

$$\begin{aligned}\sigma_{rr}|_{\partial U} &= -\mathcal{P}\chi_{[-\Theta,\Theta]}(\theta) - \tilde{\mathcal{P}}\chi_{[\pi-\tilde{\Theta},\pi+\tilde{\Theta}]}(\theta) - \mathfrak{p}\left[1-\chi_{[-\Theta,\Theta]}(\theta) - \chi_{[\pi-\tilde{\Theta},\pi+\tilde{\Theta}]}(\theta)\right] \\ &=: -\mathcal{P}'\chi_{[-\Theta,\Theta]}(\theta) - \tilde{\mathcal{P}}'\chi_{[\pi-\tilde{\Theta},\pi+\tilde{\Theta}]}(\theta) - \mathfrak{p},\end{aligned} \tag{4.44}$$

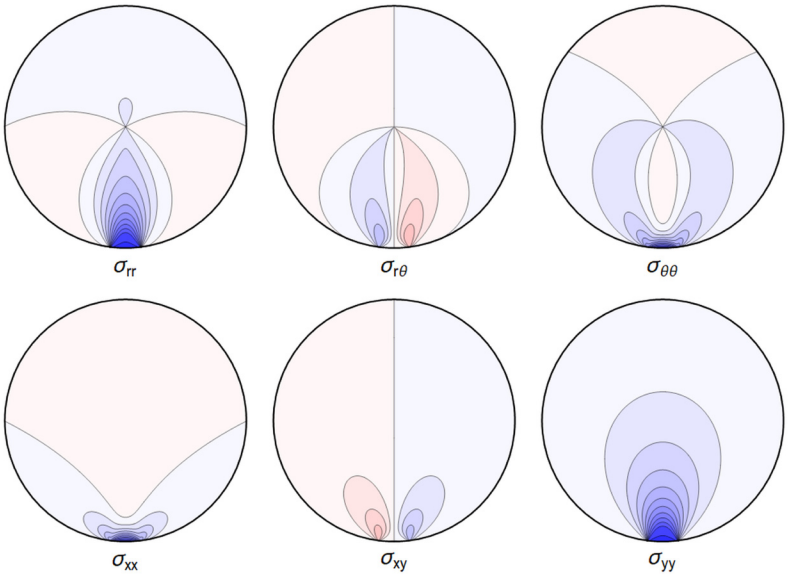


Figure 4.6. Typical internal stresses for a waveguide resting on an extended contact zone. Here, and in the following figures, we use the same parameters and the same color coding as in Figure 4.1.

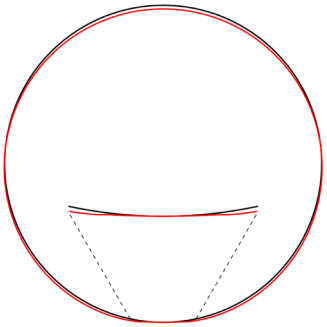


Figure 4.7. Deformation for the case of a waveguide resting on a rigid plane, drawn in red. The undeformed reference is drawn in black. Here, and in similar figures that follow, the (barely visible) indentation is an artefact of the approximation illustrated in Figure 4.5.

with Θ now an angle which approximates half of the contact region from below and $\tilde{\Theta}$ the same from above.

The Fourier coefficients for the Airy function are found to be

$$D_0 = -\frac{\mathcal{P}'\Theta + \tilde{\mathcal{P}}'\tilde{\Theta}}{2\pi} - \frac{\mathfrak{p}}{2}, \tag{4.45}$$

$$C_1 = 0, \tag{4.46}$$

$$A_n = \frac{\mathcal{P}'\sin(n\Theta) + (-1)^n\tilde{\mathcal{P}}'\sin(n\tilde{\Theta})}{\pi a^{n-2} n(n-1)}, \tag{4.47}$$

$$C_n = -\frac{\mathcal{P}'\sin(n\Theta) + (-1)^n\tilde{\mathcal{P}}'\sin(n\tilde{\Theta})}{\pi a^{n} n(n+1)}, \tag{4.48}$$

with condition Equation (3.13) giving

$$2\sin(\Theta)\mathcal{P}' = 2\tilde{\mathcal{P}}'\sin(\tilde{\Theta}) + ag\rho\pi. \tag{4.49}$$

The re-summed expression for the Airy function is

$$\phi_{\text{double}} = \phi_{\text{single}} - \frac{\tilde{\mathcal{P}}'}{2\pi}\left[r^2\left(\tilde{\Theta} + \Theta\frac{\sin(\tilde{\Theta})}{\sin(\Theta)}\right) + \xi(\theta-\tilde{\Theta}) - \xi(\theta+\tilde{\Theta}) - \frac{\sin(\tilde{\Theta})}{\sin(\Theta)}\big(\zeta(\theta-\Theta) - \zeta(\theta+\Theta)\big)\right], \tag{4.50}$$

where

$$\xi(x) \coloneqq \left[a^2 + r^2 + 2ar\cos(x)\right]\arctan\left(\frac{r\sin(x)}{a + r\cos(x)}\right). \tag{4.51}$$

All the sums converge, leading to a finite displacement field. The stresses and the displacements can be seen in Figure 4.8 and Figure 4.9 respectively. Here, and in the plots that follow, the parameters are related to those of the two contact-lines case via the correspondence

$$\tilde{\mathcal{P}}_{\text{contact line}} = \tilde{\mathcal{P}}_{\text{extended contact region}} \times 2\tilde{\Theta}, \tag{4.52}$$

which guarantees an identical integrated reaction force from the support.

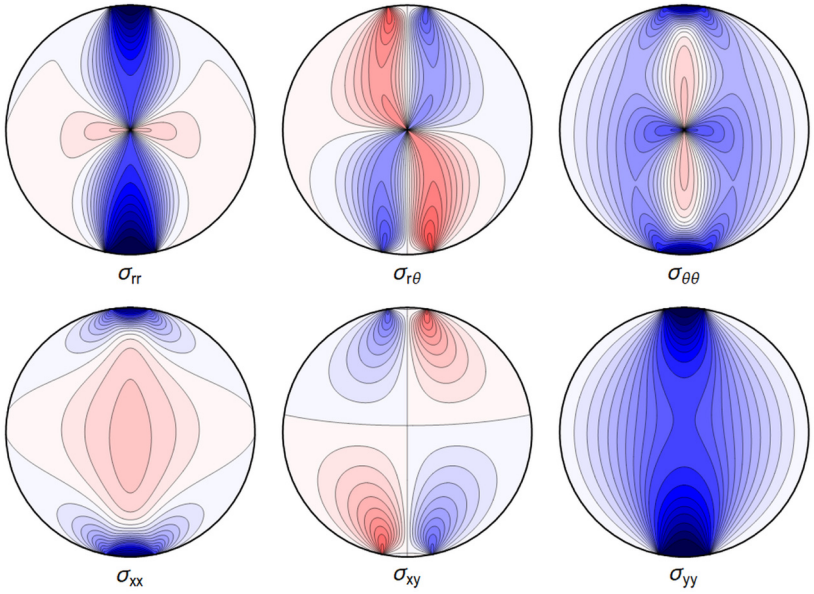


Figure 4.8. Internal stresses for the case of a waveguide squeezed between two rigid planes with extended contact region.

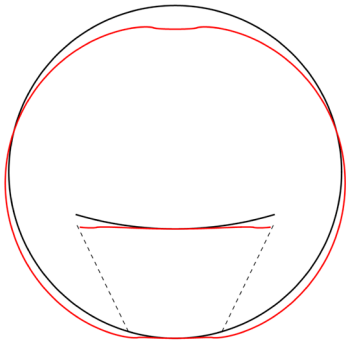


Figure 4.9. Deformation for the case of a waveguide squeezed between rigid planes of finite width, drawn in red. The undeformed reference is drawn in black.

4.2.3 Comparing models. It is of interest to compare the different contact models we employed above, in particular validating the assertion that the step-function is a good approximation for the Hertz contact pressure Equation (4.27)–Equation (4.28), at least far from the contact region. In Figure 4.10 and Figure 4.11 we show the differences between the line contact models as discussed in Section 4.1 and the step-function approximation employed in Section 4.2 going forward, for the set of parameters given in Table 4.1. In Figure 4.12 we show the difference between stresses resulting from the Hertz contact model, calculated numerically, and our explicit solution using the step-function approximation.

We can quantify the differences away from the contact points by comparing the maximal values over the regions

$$U_{1/2} = \{(r,\theta) : 0 < r \leq \frac{a}{2}, -\pi < \theta \leq \pi\} \tag{4.53}$$

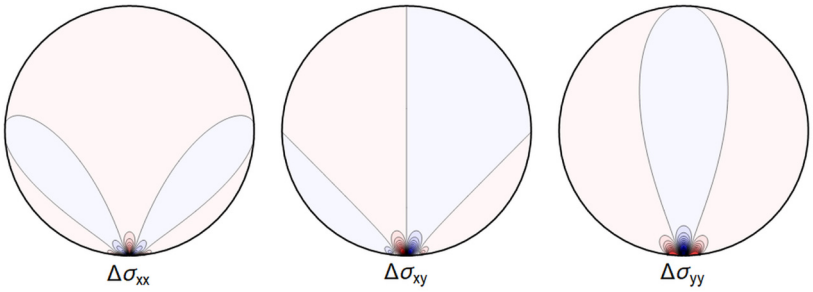


Figure 4.10. The difference $\Delta\sigma$ between the line contact Figure 4.1 and extended contact region Figure 4.6. Here and in all figures comparing two sets of stresses, shades of blue indicate negative differences, shades of red indicate positive ones, with darker colors encoding larger differences.

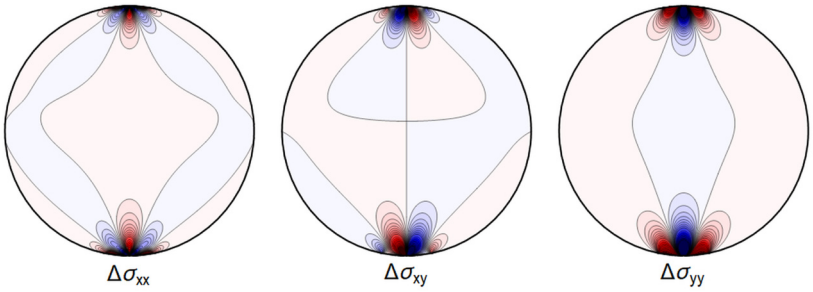


Figure 4.11. Difference $\Delta\sigma$ between the line contact of Figure 4.3 and the extended contact region of Figure 4.8. (Same color coding as in Figure 4.10).

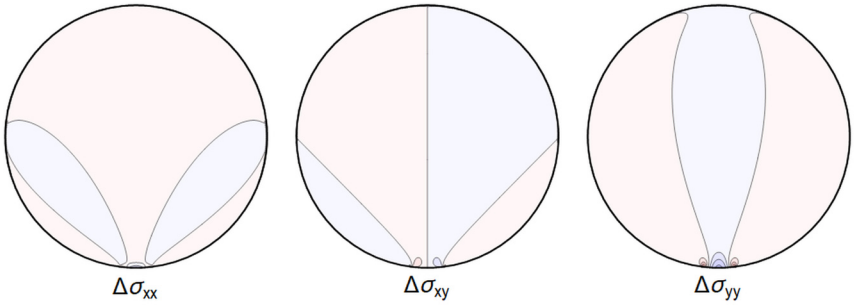


Figure 4.12. Difference $\Delta\sigma$ between the extended contact of Figure 4.6 and the stresses given by the full Hertz contact solution. (Same color coding as in Figure 4.10 and Figure 4.11).

and

$$U_{1/10} = \{(r,\theta) : 0 < r \leq \frac{a}{10}, -\pi < \theta \leq \pi\}, \tag{4.54}$$

and setting

$$\Delta_U(\sigma_1,\sigma_2) = \frac{2\max_U|\sigma_1 - \sigma_2|}{\max_U|\sigma_1| + \max_U|\sigma_2|}. \tag{4.55}$$

The results, for the parameters of Table 4.1 (used in all our figures), are shown in Table 4.2–Table 4.4.

In the case of the line-contact model, a reasonable approximation is obtained in the central region for the values of parameters considered, if a 11% error is less than the measurement errors at hand. Comparing to the Hertz contact solutions, our step-function model gives errors of ~1% close to the center. Note in addition, that the chosen parameters for visualization correspond to much larger deformations than are expected to be relevant in physical applications, leading to more significant deviations.

Of particular interest in this work is the effect on the length change given by Equation (3.17). The stress contributes to this change through the integral of its trace $\mathrm{tr}\ \sigma$ over the cross section of the body. In order to compare our models we evaluate the relative difference of the integrals over the cross-section of the trace of the stress

Table 4.2. Relative differences, as defined in Equation (4.55), between the point-contact model and our approximation of the Hertz-contact model for the model of Figure 1.3a.

	σ_{rr}	$\sigma_{r\theta}$	$\sigma_{\theta\theta}$	σ_{xx}	σ_{xy}	σ_{yy}
$\Delta_{U_{1/2}}$	2.9%	4.4%	5.5%	11.7%	6.5%	2.9%
$\Delta_{U_{1/10}}$	0.6%	1.1%	0.9%	2.5%	2.3%	0.6%

Table 4.3. Relative differences, as defined in Equation (4.55), between the point-contact model and our approximation of the Hertz-contact model for the model of Figure 1.3b.

	σ_{rr}	$\sigma_{r\theta}$	$\sigma_{\theta\theta}$	σ_{xx}	σ_{xy}	σ_{yy}
$\Delta_{U_{1/2}}$	2.4%	9.9%	7.7%	11.0%	17.2%	3.9%
$\Delta_{U_{1/10}}$	1.4%	2.0%	1.7%	5.1%	10.4%	1.5%

Table 4.4. Relative differences, as defined in Equation (4.55), between the Hertz-contact model and our step-function approximation thereof.

	σ_{rr}	$\sigma_{r\theta}$	$\sigma_{\theta\theta}$	σ_{xx}	σ_{xy}	σ_{yy}
$\Delta_{U_{1/2}}$	0.7%	1.1%	1.4%	3.0%	1.6%	0.7%
$\Delta_{U_{1/10}}$	0.2%	0.3%	0.2%	0.6%	0.6%	0.2%

tensor calculated in different models:

$$\Delta_{\int}(\sigma_1,\sigma_2) := \frac{2\left|\int_U \mathrm{tr}\sigma_1 - \int_U \mathrm{tr}\sigma_2\right|}{\left|\int_U \mathrm{tr}\sigma_1\right| + \left|\int_U \mathrm{tr}\sigma_2\right|}. \tag{4.56}$$

For the parameters listed in Table 4.1 this yields

$$\begin{aligned} \Delta_{\int}(\sigma_{\mathrm{step}},\sigma_{\mathrm{Hertz}}) &= 0.08\%, \qquad \Delta_{\int}(\sigma_{\mathrm{line}},\sigma_{\mathrm{Hertz}}) = 0.20\%, \\ \Delta_{\int}(\sigma_{\mathrm{line}},\sigma_{\mathrm{step}}) &= 0.27\%, \quad \Delta_{\int}(\sigma_{\mathrm{line}}^{\mathrm{double}},\sigma_{\mathrm{step}}^{\mathrm{double}}) = 0.21\%. \end{aligned} \tag{4.57}$$

We conclude that replacing the Hertz-contact model by a step function gives an excellent approximation, and that our simplest model, namely a contact along a line, can also be used to obtain fairly accurate numbers, for the change of length and for the deformations near the core of the waveguide, in spite of the divergence of the displacement field u at the contact line, depending upon the resolution needed.

We emphasize that this is a comparison of different contact models for a waveguide at a given height, and should not be confused with formulae such as Equation (5.2) below, where two configurations at different heights are compared using the same model.

4.2.4 Four contact regions. The calculations so far only take into account the neighbouring part of the waveguide pressing from above, ignoring the interaction between remaining neighbouring parts of the waveguide. The simplest model for this is presented in Figure 1.3c, with four contact regions for the waveguide, which we address now.

Using step-function boundary-stresses for the contact region gives

$$\sigma_{r\theta}|_{\partial U} = 0, \tag{4.58}$$

$$\begin{aligned} \sigma_{rr}|_{\partial U} &= -\mathcal{P}\chi_{[-\Theta,\Theta]}(\theta) - \tilde{\mathcal{P}}\chi_{[\pi-\tilde{\Theta},\pi+\tilde{\Theta}]}(\theta) - \bar{\mathcal{P}}\left[\chi_{[\frac{\pi}{2}-\hat{\Theta},\frac{\pi}{2}+\hat{\Theta}]}(\theta) + \chi_{[\frac{3\pi}{2}-\hat{\Theta},\frac{3\pi}{2}+\hat{\Theta}]}(\theta)\right] \\ &\quad - \mathfrak{p}\left[1 - \chi_{[-\Theta,\Theta]}(\theta) - \chi_{[\pi-\tilde{\Theta},\pi+\tilde{\Theta}]}(\theta) - \chi_{[\frac{\pi}{2}-\hat{\Theta},\frac{\pi}{2}+\hat{\Theta}]}(\theta) - \chi_{[\frac{3\pi}{2}-\hat{\Theta},\frac{3\pi}{2}+\hat{\Theta}]}(\theta)\right] \\ &=: -\mathcal{P}'\chi_{[-\Theta,\Theta]}(\theta) - \tilde{\mathcal{P}}'\chi_{[\pi-\tilde{\Theta},\pi+\tilde{\Theta}]}(\theta) - \bar{\mathcal{P}}'\left[\chi_{[\frac{\pi}{2}-\hat{\Theta},\frac{\pi}{2}+\hat{\Theta}]}(\theta) + \chi_{[\frac{3\pi}{2}-\hat{\Theta},\frac{3\pi}{2}+\hat{\Theta}]}(\theta)\right] - \mathfrak{p}, \end{aligned} \tag{4.59}$$

with Θ now an angle which approximates half of the contact region from below and $\tilde{\Theta}$ the same from above and $\hat{\Theta}$ from the sides.

The resulting Fourier coefficients in the Airy function are

$$D_0 = -\frac{\mathcal{P}'\Theta + \tilde{\mathcal{P}}'\tilde{\Theta} + 2\bar{\mathcal{P}}'\hat{\Theta}}{2\pi} - \frac{\mathfrak{p}}{2}, \tag{4.60}$$

$$C_1 = 0, \tag{4.61}$$

$$A_n = \frac{\mathcal{P}'\sin(n\Theta) + (-1)^n\tilde{\mathcal{P}}'\sin(n\tilde{\Theta}) + 2\bar{\mathcal{P}}'\cos\left(\frac{n\pi}{2}\right)\sin(n\hat{\Theta})}{\pi a^{n-2}n(n-1)}, \tag{4.62}$$

$$C_n = -\frac{\mathcal{P}'\sin(n\Theta) + (-1)^n\tilde{\mathcal{P}}'\sin(n\tilde{\Theta}) + 2\bar{\mathcal{P}}'\cos\left(\frac{n\pi}{2}\right)\sin(n\hat{\Theta})}{\pi a^{n}n(n+1)}, \tag{4.63}$$

with

$$\mathcal{P}' = \tilde{\mathcal{P}}' \frac{\sin(\tilde{\Theta})}{\sin(\Theta)} + \frac{a g \rho \pi}{2 \sin(\Theta)}, \tag{4.64}$$

as by Equation (3.13). Note in particular the absence of a term proportional to $\bar{\mathcal{P}}$ as evident by comparing to the n = 1-term in Equation (4.35). This can be physically interpreted as the sideways pressures not contributing to the force balance in the vertical direction.

All the sums converge, leading to an admissible displacement field. The stresses and the displacement can again be illustrated graphically – see Figure 4.13 and Figure 4.14.

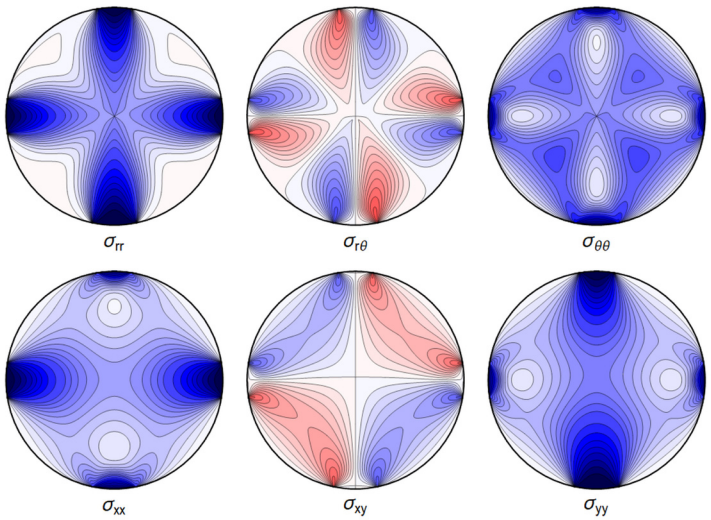


Figure 4.13. Internal stresses for the case of a waveguide squeezed between four rigid planes from below, above and the sides as depicted in Figure 1.3c, with extended contact region.

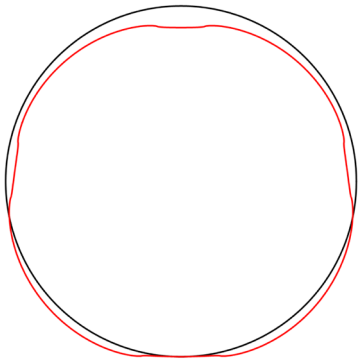


Figure 4.14. Deformation for the case of a waveguide squeezed between rigid planes of finite width as in Figure 1.3c, drawn in red. The undeformed reference is drawn in black.

4.2.5 Squeezed between six rigid planes. Our final model for spooled waveguides is given by Figure 1.3d, which we model by imposing the boundary conditions

$$\sigma_{r\theta}|_{\partial U} = 0, \tag{4.65}$$

$$\begin{aligned}\sigma_{rr}|_{\partial U} = &-\mathcal{P}\chi_{[-\Theta,\Theta]}(\theta) - \tilde{\mathcal{P}}\chi_{[\pi-\tilde{\Theta},\pi+\tilde{\Theta}]}(\theta) - \hat{\mathcal{P}}\left[\chi_{[\frac{\pi}{3}-\hat{\Theta},\frac{\pi}{3}+\hat{\Theta}]}(\theta) + \chi_{[\frac{5\pi}{3}-\hat{\Theta},\frac{5\pi}{3}+\hat{\Theta}]}(\theta)\right]\\ &- \check{\mathcal{P}}\left[\chi_{[\frac{2\pi}{3}-\check{\Theta},\frac{2\pi}{3}+\check{\Theta}]}(\theta) + \chi_{[\frac{4\pi}{3}-\check{\Theta},\frac{4\pi}{3}+\check{\Theta}]}(\theta)\right]\\ &- \mathfrak{p}\Big[1-\chi_{[-\Theta,\Theta]}(\theta) - \chi_{[\pi-\tilde{\Theta},\pi+\tilde{\Theta}]}(\theta) - \chi_{[\frac{\pi}{3}-\hat{\Theta},\frac{\pi}{3}+\hat{\Theta}]}(\theta) - \chi_{[\frac{5\pi}{3}-\hat{\Theta},\frac{5\pi}{3}+\hat{\Theta}]}(\theta)\\ &- \chi_{[\frac{2\pi}{3}-\check{\Theta},\frac{2\pi}{3}+\check{\Theta}]}(\theta) - \chi_{[\frac{4\pi}{3}-\check{\Theta},\frac{4\pi}{3}+\check{\Theta}]}(\theta)\Big]\\ = &-\mathcal{P}'\chi_{[-\Theta,\Theta]}(\theta) - \tilde{\mathcal{P}}'\chi_{[\pi-\tilde{\Theta},\pi+\tilde{\Theta}]}(\theta) - \hat{\mathcal{P}}'\left[\chi_{[\frac{\pi}{3}-\hat{\Theta},\frac{\pi}{3}+\hat{\Theta}]}(\theta) + \chi_{[\frac{5\pi}{3}-\hat{\Theta},\frac{5\pi}{3}+\hat{\Theta}]}(\theta)\right]\\ &- \check{\mathcal{P}}'\left[\chi_{[\frac{2\pi}{3}-\check{\Theta},\frac{2\pi}{3}+\check{\Theta}]}(\theta) + \chi_{[\frac{4\pi}{3}-\check{\Theta},\frac{4\pi}{3}+\check{\Theta}]}(\theta)\right] - \mathfrak{p},\end{aligned} \tag{4.66}$$

with Θ now an angle which approximates half of the contact region from below, and $\tilde{\Theta}$ the same from above, and $\hat{\Theta}$ and $\check{\Theta}$ from the sides.

The associated Fourier cosine series for the Airy functions has coefficients

$$D_0 = -\frac{\mathcal{P}'\Theta + \tilde{\mathcal{P}}'\tilde{\Theta} + 2\hat{\mathcal{P}}'\hat{\Theta} + 2\check{\mathcal{P}}'\check{\Theta}}{2\pi} - \frac{\mathfrak{p}}{2}, \tag{4.67}$$

$$C_1 = 0, \tag{4.68}$$

$$A_n = \frac{1}{\pi a^{n-2} n(n-1)}\left[\mathcal{P}'\sin(n\Theta) + (-1)^n\tilde{\mathcal{P}}'\sin(n\tilde{\Theta}) + 2\hat{\mathcal{P}}'\cos\left(\frac{n\pi}{3}\right)\sin(n\hat{\Theta}) + 2\check{\mathcal{P}}'\cos\left(\frac{2n\pi}{3}\right)\sin(n\check{\Theta})\right], \tag{4.69}$$

$$C_n = -\frac{1}{\pi a^n n(n+1)}\left[\mathcal{P}'\sin(n\Theta) + (-1)^n\tilde{\mathcal{P}}'\sin(n\tilde{\Theta}) + 2\hat{\mathcal{P}}'\cos\left(\frac{n\pi}{3}\right)\sin(n\hat{\Theta}) + 2\check{\mathcal{P}}'\cos\left(\frac{2n\pi}{3}\right)\sin(n\check{\Theta})\right], \tag{4.70}$$

with the force-balance condition Equation (3.13) leading to

$$\begin{aligned}-ag\rho &= -\frac{2}{\pi}\left(\tilde{\mathcal{P}}'\cos(\pi)\sin(\tilde{\Theta}) + 2\hat{\mathcal{P}}'\cos\left(\frac{\pi}{3}\right)\sin(\hat{\Theta}) + 2\check{\mathcal{P}}'\cos\left(\frac{2\pi}{3}\right)\sin(\check{\Theta}) + \mathcal{P}'\cos(0)\sin(\Theta)\right)\\ &= \frac{2}{\pi}\left(\tilde{\mathcal{P}}'\sin(\tilde{\Theta}) - \hat{\mathcal{P}}'\sin(\hat{\Theta}) + \check{\mathcal{P}}'\sin(\check{\Theta}) - \mathcal{P}'\sin(\Theta)\right);\end{aligned} \tag{4.71}$$

equivalently

$$\mathcal{P}' = \tilde{\mathcal{P}}'\frac{\sin(\tilde{\Theta})}{\sin(\Theta)} - \hat{\mathcal{P}}'\frac{\sin(\hat{\Theta})}{\sin(\Theta)} + \check{\mathcal{P}}'\frac{\sin(\check{\Theta})}{\sin(\Theta)} + \frac{ag\rho\pi}{2\sin(\Theta)}. \tag{4.72}$$

All the sums converge, leading to a finite displacement field. The stresses and the displacement are seen in Figure 4.15 and Figure 4.16.

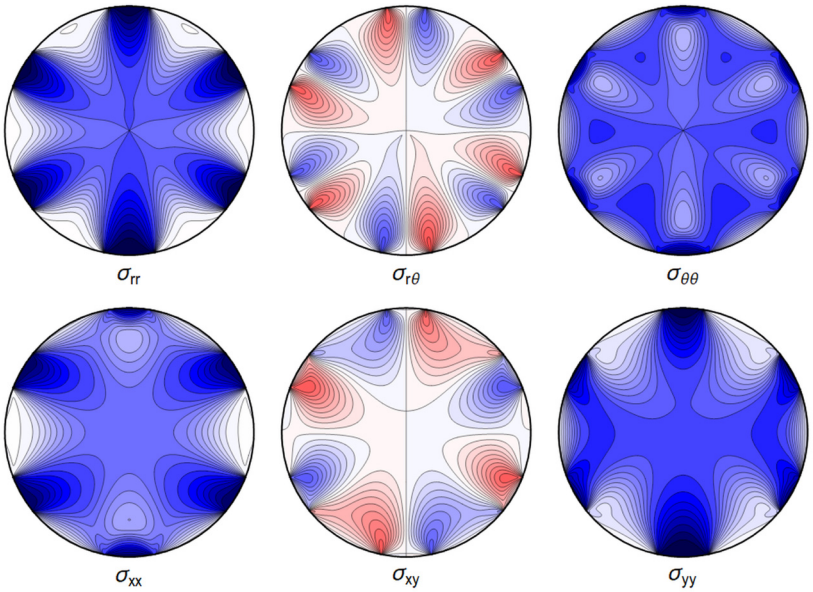


Figure 4.15. Internal stresses for the case of a waveguide squeezed between six rigid planes with extended contact regions, as in Figure 1.3d.

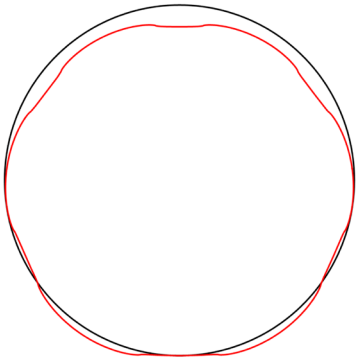


Figure 4.16. Deformation for the case of a waveguide squeezed between rigid planes of finite width as in Figure 1.3d, drawn in red. The undeformed reference is drawn in black.

5 Estimates for GRAVITES

The planned GRAVITES experiment [1] will use single-mode optical fibers made of silica glass, which we assume to be homogeneous, with material properties and experimental parameters given in Table 5.1–Table 5.2. The numbers used below, such as the change of pressure $\delta \mathfrak{p}$ and the change of temperature δT, and their outcome for the experiment, correspond to a change in height of 1 m at sea level for an unshielded experiment.

The results of our calculations make it clear that the experiment must be carried-out in a vacuum chamber, keeping in mind the following:

1. The effects scale in an obvious way with the residual pressure, in which case our calculations provide bounds on the quality of the vacuum needed for measurability of the gravitational effect.

2. The gradients of the temperature of the residual gas affect the temperature of the waveguide during the timescale of the experiment, in which case our calculations provide bounds on the residual temperature gradients.

Table 5.1. Properties of silica oxide glass from [18].

ν	E	ρ	α
0.17	73.1 GPa	2.2 g/cm^3	$1.8 \cdot 10^{-7}$ K^{-1}

Table 5.2. Parameters for GRAVITES from [1].

a	δg	δp	δT	L	β
62.5 µm	3 µm/s^2	10 Pa	10^{-2} K	10^5 m	$6 \cdot 10^6$ m^{-1}

The above can of course be circumvented by ensuring that there are neither pressure gradients nor temperature gradients, of the kind considered here, inside the vacuum chamber at the timescale of the experiment, so that the effects determined here become irrelevant. Our calculations give severe constraints on the experimental setup. It is currently planned to achieve a stability of temperature of ±20 mK at the locations of the spools, and an ambient pressure of 10^{-1} mbar for the duration of the measurement (as we cannot let the vacuum pumps run in view of the associated vibrations, and rely therefore on slow outgassing of the valved-off chamber). This means that the arms-stabilisation techniques will need to mitigate the effect of temperature changes to a level below the gravitational signal, taking into account the time scales associated with thermoelastic deformations of the waveguide.

In what follows we will need an estimate for the spooling force. The typical values for the equipment used are in the range from 0.2 to about 1 Newtons, with an accuracy of 0.05 N. We choose, in both arms,

$$F_T = 1\,\mathrm{N},$$

and we assume that this is unchanged when moving the spools in the gravitational field.

In a first very rough estimate the lateral pressures $\hat{\mathcal{P}}$ and $\check{\mathcal{P}}$, for the hexagonal case, are taken to be the same as $\bar{\mathcal{P}}$ from the quadrilateral case, as given in (A.2).

Finally, the maximal pressure $\tilde{\mathcal{P}}$ for fibers at the bottom can be estimated by the weight of the spooled fiber ~ 10 kg distributed over the area of a horizontal cross-section of the spool, resulting in

$$\tilde{\mathcal{P}}_{\max} = 1.3\,\mathrm{kPa}.$$

The actual value of $\tilde{\mathcal{P}}$ decreases with height along the spool, vanishing for the top layer.

For the following numeric estimates we use this maximal value.

In the GRAVITES experiment one interferes two photons traveling in two fibers with a typical vertical separation of 1 m. The arms of the interferometers are moved vertically during the experiment, which results in a deformation of the fiber due to a different gravitational field. The quantities that influence the measurements are the changes of deformations. Denoting by δ a change in a field, and by a bar the operation of integral averaging, we define the integral average $\delta\bar{\sigma}_{rr}$ of the difference of σ_{rr} as,

$$\delta\bar{\sigma}_{rr} := \frac{1}{\pi a^2}\int_U \Big(\sigma_{rr}(r,\theta)|_{1\,\mathrm{m}} - \sigma_{rr}(r,\theta)|_{0\,\mathrm{m}}\Big)\, r\,\mathrm{d}r\,\mathrm{d}\theta, \tag{5.1}$$

where the notation $\cdot|_h$ indicates that the quantity $\cdot$ is evaluated at a height h; analogously for $\delta\bar{\sigma}_{\theta\theta}$. We use Equation (3.17) to determine the change in the length of the fiber,

$$\delta L = L\left[-\frac{\nu}{E}(\delta\bar{\sigma}_{rr} + \delta\bar{\sigma}_{\theta\theta}) + \alpha\,\delta T\right], \tag{5.2}$$

and we use

$$\delta\varphi = \beta\delta L \tag{5.3}$$

to denote the change of phase of light due to the change of length of the waveguide.

Consider the deformation vector

$$\delta u := u|_{1m} - u|_{0m}.$$

We wish to associate to it a number which will provide information about the magnitude of the deformation, and will allow us to compare the deformation for all our models. Taking the supremum over the waveguide is not useful, since δu is infinite for the line contact models. For definiteness, and as an example, we take the supremum of the length $\|\delta u\|$ over the region $U_{1/2}$ of Equation (4.53),

$$\|\delta u\|_{\max} := \sup_{U_{1/2}} \|\delta u\|, \tag{5.4}$$

keeping in mind that the effects on light for GRAVITES are mostly relevant in the core of the waveguide.

The results are summarised in Table 5.3 for the single and double plane cases covered in Sections 4.2.1 and 4.2.2. The configurations with four and six contact planes only give small corrections compared to the two plane case, since the additional pressures are independent of the height. This should be compared with the gravitational effect

$$\boxed{\delta\varphi_{\,\mathrm{GRAVITES}} = -6.52\times10^{-5}\,\mathrm{rad}} \tag{5.5}$$

in the expected GRAVITES signal, and the hope is to attain an accuracy of 95%. The control of the temperature and the pressure needed for the GRAVITES experiment is challenging but expected to be achievable.

Let us finally note that the height of the spools will be of the order of 30 cm, so there will be gradients of $\mathfrak{p}$, T, and g along the waveguide which will influence the geometry of each arm. But, as already pointed out, in GRAVITES what matters is not the geometry itself but its change when an arm is displaced vertically. For this reason we expect that the models that we analysed suffice to provide a solid estimate of the influence of elastic deformations on GRAVITES.

It has been proposed to place the interferometer in a centrifuge, with horizontal plane of rotation, with the arms of the interferometer placed at different distances from the center of the centrifuge, achieving an acceleration gradient $\delta\mathrm{g} \approx 10$ m/s^2 between the arms. To estimate the difference of phase between the arms we invoke the equivalence principle, modelling this problem by a radial gravitational field directed away from the axis of

Table 5.3. Figures for the GRAVITES experiment. The table lists the differences in the fields resulting from a difference of height between the arms of 1 m. The columns isolate the effects with respect to their sources. We write $\delta\mathrm{g}^{\mathrm{single}}_{\mathrm{step}}$ for the effect calculated in the configuration of Section 4.2.1, $\delta\mathrm{g}^{\mathrm{single}}_{\mathrm{line}}$ for the effect calculated in the configuration of Section 4.1.1, and $\delta\mathrm{g}^{\mathrm{double}}_{\mathrm{step}}$ for that in Section 4.2.2; $\delta\overline{\sigma}_{rr}$ is defined in (5.1); $\|\delta u\|_{\max}$ is the maximal transverse deformation of the waveguide over the region $U_{1/2}$ defined in Equation (4.53); δL is the change of length of the waveguide due to the Poisson effect; $\delta\varphi$ is the change of phase of light due to the elastic elongation of the waveguide.

	$\delta\mathbf{g}^{\mathbf{single}}_{\mathbf{step}}$	$\delta\mathbf{g}^{\mathbf{single}}_{\boldsymbol{line}}$	$\delta\mathbf{g}^{\boldsymbol{double}}_{\mathbf{step}}$	$\delta\mathfrak{p} = 10$ Pa	$\delta T = 10^{-2}$ K
$\delta\overline{\sigma}_{rr}$[Pa]	$2.1\cdot10^{-7}$	$2.1\cdot10^{-7}$	$2.9\cdot10^{-7}$	10	0
$\|\delta u\|_{\max}$[μm]	$8.5\cdot10^{-15}$	$7.2\cdot10^{-15}$	$9.9\cdot10^{-15}$	$9.9\cdot10^{-9}$	$2.0\cdot10^{-7}$
δL[μm]	$9.6\cdot10^{-8}$	$1.3\cdot10^{-7}$	$1.3\cdot10^{-7}$	4.7	180
$\delta\varphi$[rad]	$5.8\cdot10^{-7}$	$7.9\cdot10^{-7}$	$8.0\cdot10^{-7}$	28	1080

rotation of the centrifuge, with strength depending upon the distance from the axis, and ignoring the Earth gravitational field which acts with constant strength normal to the plane of rotation. (Clearly a more precise model would be needed for the real experiment. For example, the gradient of the "gravitational field" along the length of the spool is likely to become relevant; the deformations of the supporting elements might have to be taken into account.) For future reference, the corresponding values are given in Table 5.4; we do not include effects related to the change of temperature or pressure there, as such effects would depend strongly upon the experimental setup.

A Relation between $\bar{\mathcal{P}}$ and κ

The pressure terms $\bar{\mathcal{P}}$ in the quadrilateral configuration, as well as $\hat{\mathcal{P}}$ and $\check{\mathcal{P}}$ in the hexagonal configuration are linked to the spooling tension. We make this relation explicit for the case of a waveguide pressing against a rigid cylinder of radius R.

We assume a static configuration, and we ignore boundary effects at the point where the contact between the waveguide and the spool is lost. We consider a waveguide, consisting of an optical fiber, which is wound N times in one layer around a rigid cylinder of radius R. We suppose that the contact interface of the waveguide and the cylinder has constant width w, and that the pressure, which we denote by $\bar{\mathcal{P}}$, exerted on the cylinder by the waveguide is constant across the whole area of contact. We assume that the axis of the cylinder is vertical, and we are interested in the pressure felt by the waveguide at the contact interface between the waveguide and the cylinder.

In a real-life situation there would be several layers of the waveguide, with various radii, with only the lowest one in contact with the cylinder, and the further ones in contact with neighbouring layers. Here we only consider the first layer, which is in contact with the cylinder. Similar considerations can be applied to describe successive layers; one would then also need to take into account the fact that the neighbouring layers are elastic and not rigid, as well as deformations of the neighbouring layers arising from the Poisson ratio. Our analysis in the main body of the paper sets the ground for further such investigations, which are left to future work.

We relate the pressure $\bar{\mathcal{P}}$ of Figure 1.3c to the tension force F_T by considering the free-body diagram of a half of a single turn of a waveguide, i.e., we consider the intersection of the spool together with the waveguide and a plane on which the axis of the spool lies. The left Figure A.2 shows the intersection when viewed from above the spool of Figure A.1.

Let us imagine that we have a constant pressure $\bar{\mathcal{P}}$ acting from the side as in Figure 1.3c, generating a force orthogonal to the contact region with the spool. This pressure generates a force $\mathcal{F}$ which should equate the tension forces, i.e., $\mathcal{F} = 2F_T$, where

$$\mathcal{F} := \int_{-\pi/2}^{\pi/2} \bar{\mathcal{P}} \cos\varphi \mathcal{A} \, \mathrm{d}\varphi = 2Rw \int_{-\pi/2}^{\pi/2} \bar{\mathcal{P}} \cos\varphi \, \mathrm{d}\varphi \tag{A.1}$$

is the normal force due to the pressure $\bar{\mathcal{P}}$ acting on the contact area $\mathcal{A}$ and φ is the angle shown in Figure A.2 cover 180 degrees of a semicircle. Hence, $\mathcal{F}$ is the effective force caused by the pressure $\bar{\mathcal{P}}$.

Table 5.4. Estimates for a centrifuge experiment with $\delta g = 10$ m/s² at one meter separation. Notation as in Table 5.3.

	$\delta g_{\text{step}}^{\text{single}}$	$\delta g_{\text{step}}^{double}$
$\delta\bar{\sigma}$[Pa]	0.7	1.5
$\lVert\delta u\rVert_{\max}$[µm]	$2.4 \cdot 10^{-8}$	$4.0 \cdot 10^{-8}$
δL[µm]	0.3	0.7
$\delta\varphi$[rad]	1.9	4.2

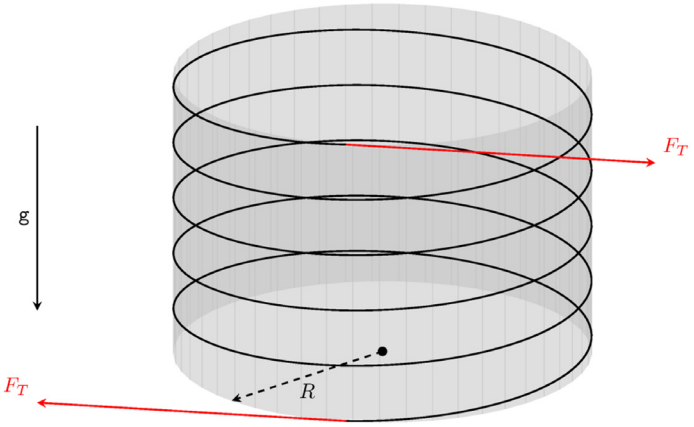


Figure A.1. A waveguide wound around a rigid cylinder with radius R. We show a single layer of waveguide wrapped around the spool. Equal tension forces are applied at both the starting and end points so that the spool is in equilibrium. The spacing between the neighboring sections of the fiber has been increased for visual clarity.

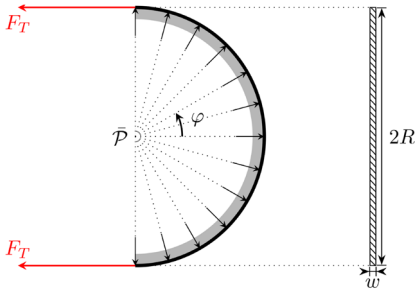


Figure A.2. Free-body diagram of half of a single turn of waveguide around the spool (this corresponds to a view from above in Figure 1.3c or Figure A.1, so that the vertical is orthogonal to the plane of the picture). The rectangle on the right-hand side shows the contact area with the width w as viewed from the left. The arrows illustrate the direction of the (uniform) reaction force.

We assume that the tension force is constant along the waveguide. Therefore, we find $\mathcal{F} = 4Rw\bar{\mathcal{P}}$, which after equating the forces yields

$$\bar{\mathcal{P}} = \frac{F_T}{2Rw}. \tag{A.2}$$

Recall that the constant $\mathbb{F}$ appearing in the Hertz constant problem is defined as the total force per unit length pushing the bodies into each other, which in our context translates to $\bar{\mathcal{P}} = \mathbb{F}/w$. Comparing with (A.2) we find

$$\mathbb{F} = \frac{F_T}{2R}. \tag{A.3}$$

(Note that this is independent of the number of windings in the spool, and that a virtual work calculation gives the same result.) This value of $\mathbb{F}$ can now be used in Section 4.2 to calculate w by solving the contact problem.

This formula is valid for the first layer, as counted starting from the core of the spool. One can generalize the result for the case where we have more layers that exert forces upon each other by writing

$$\bar{\mathcal{P}}_n - \bar{\mathcal{P}}_{n+1} = \frac{F_T}{2[R+(n-1)a]w_n}, \tag{A.4}$$

where w_n is the contact width at the n'th layer, while $\bar{\mathcal{P}}_n$ and $\bar{\mathcal{P}}_{n+1}$ are the contact pressures there.

B Extending to non-symmetric solutions

Although the mirror symmetry assumption made in Section 2 is well-motivated for our purposes, we nevertheless give the full solution for completeness, demanding only regularity at $r = 0$ and 2π-periodicity in θ.

Discarding only terms incompatible with regularity and 2π-periodicity in (2.26), as well as B_0, D_1 and d_1 which do not contribute to the stresses, we have

$$\begin{aligned}\phi(r,\theta) = {} & D_0 r^2 + C_1 r^3 \cos(\theta) + c_1 r^3 \sin(\theta) \\ & + \sum_{n\geq 2} \Big[\left(A_n r^n + C_n r^{n+2} \right) \cos(n\theta) + \left(a_n r^n + c_n r^{n+2} \right) \sin(n\theta) \Big].\end{aligned} \tag{B.1}$$

Again, the displacement can be derived by integrating (2.22)–(2.24), yielding

$$\begin{aligned}u_r(r,\theta) = \frac{1}{2\mu} \Big\{ & 2(1-2\nu) D_0 r - \frac{1}{2} g\rho (1-2\nu) r^2 \cos(\theta) + (1-4\nu) r^2 (C_1 \cos(\theta) + c_1 \sin(\theta)) \\ & + \sum_{n\geq 2} \Big(\left[-n A_n r^{n-1} + (2-4\nu-n) C_n r^{n+1} \right] \cos(n\theta) \\ & + \left[-n a_n r^{n-1} + (2-4\nu-n) c_n r^{n+1} \right] \sin(n\theta) \Big) \Big\} \\ & - \Xi \cos(\theta) + \Xi_2 \sin(\theta) - \nu\kappa r + (1+\nu)\, \alpha (T - T_0) r,\end{aligned} \tag{B.2}$$

$$\begin{aligned}u_\theta(r,\theta) = \frac{1}{2\mu} \Big\{ & (5-4\nu) r^2 (C_1 \sin(\theta) + c_1 \cos(\theta)) - \frac{1}{2} g\rho (1-2\nu) r^2 \sin(\theta) \\ & + \sum_{n\geq 2} \Big(\left[n A_n r^{n-1} + (4-4\nu+n) C_n r^{n+1} \right] \sin(n\theta) \\ & + \left[-n a_n r^{n-1} - (4-4\nu+n) c_n r^{n+1} \right] \cos(n\theta) \Big) \Big\} \\ & + \Xi \sin(\theta) + \Xi_2 \cos(\theta) + c^* r,\end{aligned} \tag{B.3}$$

with the integration constants determined by the boundary conditions $u_r(a, 0) = 0 = u_\theta(a, 0)$ as above. Thus,

$$\begin{aligned}\Xi = \frac{1}{2\mu} \Big\{ & 2(1-2\nu) D_0 a + (1-4\nu) C_1 a^2 - \frac{1}{2} g\rho (1-2\nu) a^2 \\ & + \sum_{n\geq 2} \left[-n A_n a^{n-1} + (2-4\nu-n) C_n a^{n+1} \right] \Big\} - \nu\kappa a + (1+\nu)\, \alpha (T - T_0) a,\end{aligned} \tag{B.4}$$

and further

$$\Xi_2 = \frac{1}{2\mu} \left\{ (5-4\nu) a^2 c_1 + \sum_{n\geq 2} \left[n a_n a^{n-1} + (4-4\nu+n) c_n a^{n+1} \right] \right\} - c^* a, \tag{B.5}$$

provided that the sums converge.

Continuing to the boundary conditions, we immediately restrict to the frictionless case, taking

$$\sigma_{r\theta}|_{\partial U} = 0. \tag{B.6}$$

The boundary condition for σ_{rr} can now be a general Fourier series which we write in the suggestive form

$$\sigma_{rr}|_{\partial U} = f(\theta) = f_0 + \sum_{n\geq 1} [(f_{-n} + f_n) \cos(n\theta) + i (f_{-n} - f_n) \sin(n\theta)], \tag{B.7}$$

with

$$f_n = \frac{1}{2\pi}\int_{-\pi}^{\pi} \mathrm{d}\theta\, f(\theta)\, e^{in\theta}. \tag{B.8}$$

These boundary conditions determine the coefficients in (B.1) algebraically by comparing to the corresponding stresses (2.15)–(2.17). We find

$$C_1 = c_1 = 0,\ C_n = \frac{1-n}{a^2(1+n)} A_n \text{ and } c_n = \frac{1-n}{a^2(1+n)} a_n, \tag{B.9}$$

via (B.6), leading to

$$\sigma_{rr}|_{\partial U} = 2D_0 - a\mathrm{g}\rho\cos(\theta) + \sum_{n\geq 2} 2(1-n)a^{n-2}[\sin(n\theta)a_n + \cos(n\theta)A_n], \tag{B.10}$$

and comparing with (B.7) for the remaining coefficients

$$D_0 = \frac{1}{2} f_0, \tag{B.11}$$

$$A_n = -\frac{1}{2(n-1)} a^{2-n}(f_{-n} + f_n), \tag{B.12}$$

$$a_n = -\frac{i}{2(n-1)} a^{2-n}(f_{-n} - f_n), \tag{B.13}$$

for $n \geq 2$, as well as

$$f_{-1} + f_1 = -a\mathrm{g}\rho, \tag{B.14}$$

$$f_{-1} - f_1 = 0. \tag{B.15}$$

Note that, similarly to the symmetric case the space of possible boundary conditions is constrained by the body force. Without any body forces oriented along the x-direction (B.15) requires that the $\sin(\theta)$ term in (B.7) vanishes.

In the simplest case, considering line forces from the left and right and a line support from the bottom, i.e. boundary conditions

$$\sigma_{r\theta}|_{\partial U} = 0, \tag{B.16}$$

$$\sigma_{rr}|_{\partial U} = -\mathcal{P}\delta(\theta) - \hat{\mathcal{P}}\delta(\theta - \pi/2) - \check{\mathcal{P}}\delta(\theta + \pi/2), \tag{B.17}$$

Equation (B.15) implies $\hat{\mathcal{P}} = \check{\mathcal{P}}$, thus forcing mirror symmetry.

Data availability

No data are associated with this article.

Acknowledgements

Useful discussions with Thomas Mieling and Philip Kornreich are acknowledged. We are very grateful to Robert Beig, Michele Brun, Matthew Maitra, and Arash Yavari for advice and comments about previous versions of the manuscript. Research of P.T.C. and E.S. was supported in part by the Austrian Science Fund (FWF), Project P34274 and by the European Union (ERC, GRAVITES, project no 101071779). H.B. was supported in part by the European Research Council (ERC) under the European Union's Horizon 2020 research and innovation program (grant agreement ERC advanced grant 740021–ARTHUS, PI: Thomas Buchert). Views and opinions expressed are however those of the authors only and do not necessarily reflect those of the European Union or the European Research Council Executive Agency. Neither the European Union nor the granting authority can be held responsible for them.

A previous version of this submission is available as a preprint here: https://arxiv.org/pdf/2401.16949.pdf.

References

1. Hilweg C, Massa F, Martynov D, *et al.*: **Gravitationally induced phase shift on a single photon.** *New J Phys.* 2017; **19**: 033028.
Publisher Full Text
2. Beig R: **Relativistic elasticity II.** *Class Quant Grav.* 2023; **40**(8): 084001.
Publisher Full Text
3. Beig R, Schmidt BG: **Relativistic elasticity.** *Class Quant Grav.* 2003; **20**(5): 889.
Publisher Full Text
4. Carter B, Quintana H: **Foundations of general relativistic high-pressure elasticity theory.** *Proc R Soc Lond Ser A.* 1972; **331**(1584): 57–83.
Publisher Full Text
5. Kijowski J, Magli G: **Relativistic elastomechanics as a lagrangian field theory.** *Journal of Geometry and Physics.* 1992; **9**(3): 207–223.
Publisher Full Text
6. Marsden J, Hughes TJR: **Mathematical foundations of elasticity**. Dover Publications, Inc, 1994.
Reference Source
7. Hudelist M, Mieling TB, Palenta S: **Relativistic theory of elastic bodies in the presence of gravitational waves.** *Class Quant Grav.* 2023; **40**(8): 085007.
Publisher Full Text
8. Steininger E, Mieling TB: **Elastically induced phase-shift and birefringence in optical fibers**. in preparation.
9. Sadd MH: **Elasticity: theory, applications and numerics**. second edition ed., Academic Press, 2009.
10. Landau LD, Lifshitz EM: **Theory of elasticity. Course of theoretical physics**. Elsevier Butterworth-Heinemann, 1986; 7.
11. Zhenye W, Shiping L: **The generalized plane strain problem and its application in three-dimensional stress measurement.** *International Journal of Rock Mechanics and Mining Sciences & Geomechanics Abstracts.* 1990; **27**(1): 43–49.
Publisher Full Text
12. Gould PL: **Introduction to linear elasticity**. 3rd ed. 2013. ed., Springer New York, 2013.
Publisher Full Text
13. Airy GB: **On the strains in the interior of beams.** *Philos Trans R Soc London.* 1863; **153**: 49–79.
Publisher Full Text
14. Barber JR: **Elasticity**. Springer Netherlands, 2010.
Publisher Full Text
15. Michell JH: **On the direct determination of stress in an elastic solid, with application to the Theory of Plates.** *Proc Lond Math Soc.* 1899; **s1–31**(1): 100–124.
Publisher Full Text
16. Timoshenko S, Goodier JN: **Theory of Elasticity**. second ed., McGraw-Hill, 1951.
17. Hertz H: **On the contact of rigid elastic solids and on hardness**. Ch 6: Assorted Papers, 1882.
Reference Source
18. Crystran Ltd: **Silica glass (sio2).** Data Sheet published online, 2012.

Open Peer Review

Current Peer Review Status: ✔ ✔ ? ✔

Version 2

Reviewer Report 24 December 2024

https://doi.org/10.21956/openreseurope.20364.r48085

© **2024 Svetlizky I.** This is an open access peer review report distributed under the terms of the Creative Commons Attribution License, which permits unrestricted use, distribution, and reproduction in any medium, provided the original work is properly cited.

✔ **Ilya Svetlizky**
Physics department, Technion Israel Institute of Technology (Ringgold ID: 26747), Haifa, Haifa District, Israel

Review of “On elastic deformations of cylindrical bodies under the influence of the gravitational field” Barzegar et al.

This paper explores the elastic deformation of optical waveguides under the combined influences of gravitational fields, temperature, and external pressure, motivated by experiments investigating the impact of gravity on photon propagation in optical fibers. The authors model the spooled waveguide as multiple straight and parallel cylinders. The contact between the cylinders is modeled by either a singular line or a more realistic uniformly distributed pressure. Using the classical Michell series, the authors obtain analytical estimates of the stresses within the waveguide and compare these to the numerical solutions based on the Hertzian contact boundary conditions. These findings hold significant importance for interpreting experimental data from the GRAVITES experiment.

I find the manuscript to be well-written. The authors provide a comprehensive introduction—making the text self-contained—and a detailed discussion of the analysis, which appears to be sound. Additionally, the authors thoroughly address previous referees' constructive feedback, enhancing their work's robustness and clarity. For these reasons, I recommend this article for indexing.

Is the work clearly and accurately presented and does it cite the current literature?
Yes

Is the study design appropriate and does the work have academic merit?
Yes

Are sufficient details of methods and analysis provided to allow replication by others?
Yes

If applicable, is the statistical analysis and its interpretation appropriate?
Not applicable

Are all the source data underlying the results available to ensure full reproducibility?
Yes

Are the conclusions drawn adequately supported by the results?
Yes

Competing Interests: No competing interests were disclosed.

Reviewer Expertise: Experimental soft condensed matter physics

I confirm that I have read this submission and believe that I have an appropriate level of expertise to confirm that it is of an acceptable scientific standard.

Reviewer Report 16 December 2024

https://doi.org/10.21956/openreseurope.20364.r48026

© 2024 Maitra M. This is an open access peer review report distributed under the terms of the Creative Commons Attribution License, which permits unrestricted use, distribution, and reproduction in any medium, provided the original work is properly cited.

Matthew Maitra
ETH Zurich, Zürich, Zurich, Switzerland

My thanks to the authors for making these revisions. Right now I have nothing more to add.

Is the work clearly and accurately presented and does it cite the current literature?
Yes

Is the study design appropriate and does the work have academic merit?
Yes

Are sufficient details of methods and analysis provided to allow replication by others?
Yes

If applicable, is the statistical analysis and its interpretation appropriate?
Yes

Are all the source data underlying the results available to ensure full reproducibility?
Yes

Are the conclusions drawn adequately supported by the results?
Yes

Competing Interests: No competing interests were disclosed.

Reviewer Expertise: Theoretical continuum mechanics; theoretical seismology; magnetohydrodynamics

I confirm that I have read this submission and believe that I have an appropriate level of expertise to confirm that it is of an acceptable scientific standard.

Version 1

Reviewer Report 23 August 2024

https://doi.org/10.21956/openreseurope.18729.r41793

© **2024 Brun M.** This is an open access peer review report distributed under the terms of the Creative Commons Attribution License, which permits unrestricted use, distribution, and reproduction in any medium, provided the original work is properly cited.

?

Michele Brun
[1] University of Cagliari, Cagliari, Italy
[2] University of Cagliari, Cagliari, Italy

The paper presents some semi-analytical results for an elongated cylinder subjected to a transverse gravitational load and various contact forces.

The study is motivated by the need to model a planned experiment that aims to explore the influence of the gravitational field on entangled photons propagating in waveguides.

The approach used is classical and well-executed, determining the solutions in terms of Airy potentials. However, the advantage of this solution is currently limited by the availability of numerical techniques, particularly in the linear regime. Nonetheless, the work has its validity. The proposed results can be considered as an application of existing techniques to a specific problem.

Overall, I believe the work deserves acceptance after the following minor revisions have been addressed:

1. The authors refer to large elastic deformations in the Background section, but the entire model has been developed in the small deformation (geometrically linear) regime.
2. Figure 1.1 is not sufficiently explanatory for a non-specialist, and additional details should be included. It is strongly recommended to visualize the reference system in most of the figures.
3. Page 4, Section 2: expression (2.1) is not specific to an isotropic homogeneous material, but rather to a linear isotropic material. Note that inhomogeneity only implies that material constants are functions of position.
4. The approximation indicated in Figure 4.5 is not validated. Would considering a piecewise constant approximation with additional subintervals for the pressure distribution improve

the precision of the solution? In this regard, it should also be noted that the difference formula (4.50) is based on solutions that are relatively far from the load application neighborhoods.

5. I think that formula (4.64) is not correct since it appears has a linear momentum balance along y-direction and the components of the radial stresses resultants should be considered.
6. In eqns. (5.1) and (5.2) the notation @ is not explained.
7. In Appendix a the second \bar\mathcal{P} should be \hat\mathcal{P}.
8. I do not understand the factor 2 on the right handside of eqn. (A.1). Following classical Mariotte formula the 2 should be absent.
9. In the figure where contour plots of stress fields are shown legends should be inserted. These are of particular importance in Fig. 4.10.

In conclusion I think that the work can be indexed after a revision.

Is the work clearly and accurately presented and does it cite the current literature?
Yes

Is the study design appropriate and does the work have academic merit?
Partly

Are sufficient details of methods and analysis provided to allow replication by others?
Yes

If applicable, is the statistical analysis and its interpretation appropriate?
Not applicable

Are all the source data underlying the results available to ensure full reproducibility?
Yes

Are the conclusions drawn adequately supported by the results?
Yes

Competing Interests: No competing interests were disclosed.

Reviewer Expertise: Solid Mechanics

I confirm that I have read this submission and believe that I have an appropriate level of expertise to confirm that it is of an acceptable scientific standard, however I have significant reservations, as outlined above.

Author Response 28 Oct 2024

Elisabeth Steininger

We are grateful to the referee for his careful reading of our paper, and for helpful suggestions which led to significant improvements of our manuscript. We address the

changes made in response to the comments (reproduced in italics) point by point:

1) *The authors refer to large elastic deformations in the Background section, but the entire model has been developed in the small deformation (geometrically linear) regime.*
Author response: We changed the background paragraph accordingly, and expanded it somewhat.

2) *Figure 1.1 is not sufficiently explanatory for a non-specialist, and additional details should be included. It is strongly recommended to visualize the reference system in most of the figures.*
Author response: We considerably expanded the caption following the recommendation. We are using the y-axis as the vertical direction in all the calculations, which we emphasised in the new caption, and we are using the y-axis accordingly in all Figures except Fig A.2. We have added the direction of the gravitational force in Figure 2.2 and A.1, and we propose not to add this information to those remaining Figures where it is not already available.

3) *Page 4, Section 2: expression (2.1) is not specific to an isotropic homogeneous material, but rather to a linear isotropic material. Note that inhomogeneity only implies that material constants are functions of position.*
Author response: (The equation has number 2.2 now) Removed the implication that the expression describes a homogeneous material. Stated afterwards that we restrict to homogeneous materials by taking the material parameters to be constant.

4) *The approximation indicated in Figure 4.5 is not validated. Would considering a piecewise constant approximation with additional subintervals for the pressure distribution improve the precision of the solution? In this regard, it should also be noted that the difference formula (4.50) is based on solutions that are relatively far from the load application neighbourhoods.* **Author response:** We have added a comparison between the exact Hertz model, calculated by numerical methods and our step function approximation, which allows an explicit formula. A table and figure showing the differences has been added.

5) *I think that formula (4.64) is not correct since it appears has a linear momentum balance along y-direction and the components of the radial stresses resultants should be considered.*
Author response: (The equation has number 4.75 now) We have added an explicit calculation, which makes clear how the equations fits the radial stresses resultant; it was indeed confusing, as the cos of some angles involved are 1/2 or -1/2, and some of the pressures enter twice.

6) *In eqns. (5.1) and (5.2) the notation @ is not explained.*
Author response: Deleted the @ notation since it is superfluous, and added an explanation of the notation used.

7) *In Appendix a the second $\overline{\mathcal{P}}$ should be $\hat{\mathcal{P}}$.*
Author response: Fixed.

8) *I do not understand the factor 2 on the right handside of eqn. (A.1). Following classical Mariotte formula the 2 should be absent.*
Author response: The factor 2 appears because $\mathcal F$ equals $2F_T$.

9) *In the figure where contour plots of stress fields are shown legends should be inserted. These are of particular importance in Figure 4.10.*
Author response: The explanation of color coding in Figure 4.1 has been made clearer. We also added an explanation of the color coding in the caption of Figure 4.10.

Competing Interests: No competing interests were disclosed.

Reviewer Report 27 July 2024

https://doi.org/10.21956/openreseurope.18729.r41521

© 2024 Maitra M. This is an open access peer review report distributed under the terms of the Creative Commons Attribution License, which permits unrestricted use, distribution, and reproduction in any medium, provided the original work is properly cited.

?

Matthew Maitra
[1] ETH Zurich, Zürich, Zurich, Switzerland
[2] ETH Zurich, Zürich, Zurich, Switzerland

SUMMARY

This paper investigates how the thermo-elastic deformation of an optical fibre will impact the phase-shift of photons passing through it. The paper supports the GRAVITES experiment -- a project that seeks to determine how Earth's gravity affects entangled photons -- by deriving some `extra' effects that will need to be corrected for when analysing the experimental data.

The GRAVITES experiment will essentially be an interferometer (placed in a vacuum chamber) whose two arms are optical fibres spaced a vertical metre apart. Entangled photons will pass through those arms, and the phase shift between the two arms will be measured. However, the two arms are expected to undergo different thermo-elastic deformations due to the differences in gravity, pressure and temperature between the arms. Crucially, this could lead to a change in the length of the arms, which would in turn lead to an extra phase-shift between the photons that would need to be corrected for. Ultimately, this change in length is the crucial quantity that the present paper seeks to derive.

This paper therefore studies the thermo-elastic deformation of a long, homogenous, isotropic cylinder; the cylinder is clamped at one end and a force F_{T} is applied to the other, with the other external forces acting on the cylinder being ambient pressure and its own weight. The cylinder represents each of the arms of the interferometer. In reality the fibres will be spooled, but the authors argue (quite reasonably) that the radius of the spool will be so much larger than the the radius of the fibre that one may reasonably analyse instead the deformation of a long, straight cylinder subject to a `spooling tension force' (F_{T}).

In Section 2 the authors state and solve the equations of static (thermo-)elastic deformation, first

reducing the dimensionality of the problem by taking the cylinder's along-axis deformation to be precisely linear in z (eq. 2.5), then using the Airy stress-function to write down a general solution. In Section 3 they state the boundary conditions, as well as the crucial result (eq. 3.17) concerning the relationship between external parameters and the fibre's overall elongation. They match their solution to the boundary conditions for a variety of different representative geometries in Section 4, before discussing the application of their results to GRAVITES in Section 5.

The paper's language is clear and its analysis seems sound -- I appreciated Section 4's figures and adaptation of Hertz' method -- but I found the overall structure and aims quite hard to grasp. Multiple readings were required before I actually understood what Table 5.3 is saying (assuming I have now come to a correct understanding!). In what follows I will therefore mainly focus on structure and notation.

DISCUSSION

1
Please lead the reader more clearly through the analysis, stating clearly why certain equations are being derived and certain assumptions made:

1a
As discussed above (and hopefully my interpretation is correct) the crucial relationship derived in the paper is eq.(3.17). But the authors do not flag the importance of this relationship explicitly, nor is eq.(3.17) even *referenced* in Section 5 when the GRAVITES estimates are made! Please make sure that this equation's importance is emphasised, and that its centrality to equations (5.1),(5.2),(5.3) -- and thus to the whole paper -- is stated.

1b
In that connection, please make EXPLICIT that Table 5.3 refers to DIFFERENCES BETWEEN THE RESPECTIVE INTERFEROMETER ARMS. It might be obvious after a few readings of the paper -- and I have little doubt that it is trivial to people who have immersed themselves in this topic for months -- but I don't think that the present manuscript makes clear what is being compared to what. I would appreciate something like the following to be added to the end of Section 3, after eq.(3.17): ``Given a spooling force and upon specifying ambient gravity, pressure and temperature, eq.(3.17) allows the computation of the elongation of an optical fibre, that is of each arm of the interferometer. Now, due to the arms' one-metre vertical spacing, the ambient variables could be different for each arm; the spooling force could be different too because two different spools will be used. We should therefore expect each arm of the interferometer to be of different length. This difference in length will lead to an extra phase-shift that must be corrected for and that is derived directly from eq.(3.17). In Section 4 we proceed to derive expressions for \sigma_{xx} and \sigma_{yy} in terms of ambient pressure and gravity, so that eq.(3.17) can indeed be seen to express a relationship between each arm's actual length and: p,T,g and F_{T}.''
If words to this effect had been included in the manuscript (perhaps even in the Introduction) I think I would have had a *much* easier time understanding where things were going.

1c
Please introduce and describe the spooling force F_{T} earlier in the main text, rather than just mentioning it in passing in the caption of Figure 2.1c. Preferably, state at the beginning of Section 2 that the model of the waveguide that this paper analyses in detail is the version from Figure 2.1c, and that we therefore have displacement-free boundary conditions on one end while needing to match the stress at the other end to the externally imposed force F_{T}. Incidentally, this would give a much clearer motivation for imposing eq.(2.5) than what the manuscript offers at present.

1d
Following on directly from 1c, please motivate eq.(2.5) more clearly (I didn't find the statement "compare Figure 2.1 (a)–(c)" to help much in that regard). Once the spooling force has been foregrounded, this should be easy. In addition, I would appreciate a note after eq.(2.10) stating that the z-component of the force-balance equation is automatically satisfied.

1e (miscellaneous)
Eq.(2.1):
What are \sigma and \epsilon?! A reader without much background in elasticity would be stuck here; please define all terms used in the paper. In addition, eq.(2.6) should logically precede eq.(2.1): how can you define strain without any concept of deformation? Also, the material need not be homogeneous for eq.(2.1) to hold.
Eq.(2.11):
\sigma_{rr} + \sigma_{\theta\theta} should probably read \sigma_{xx} + \sigma_{yy} because the cylindrical coordinate system has not yet been introduced.
Eq.(4.32):
Please define both `A' and the concept of `indicator function'. (Presumably A here is different from the A in equations (4.10), (4.11) and (4.12)?!)
Eq.(5.3):
\delta\overline{\sigma}_{\theta\theta} has not yet been formally defined. Eq.(5.1) should be adjusted to include this definition.

2
Temperature and thermo-elasticity.
A temperature T_{0} is introduced in eq.(2.3) as a `baseline', with T being the actual (constant) temperature of the optical fibre. Assuming that \delta{T} in Table 5.3 represents the difference between the *actual* temperatures of the interferometer's respective arms, then eq.(5.3) should have (T-T_{0}) replaced by \delta{T}. (This caused me a lot of confusion at first!)

3
I would like to see more uncertainty estimates, please.

3a
What is the rough uncertainty on the spooling force. How different will it therefore be between the two arms?

3b
What is the rough uncertainty on phase-shift due to gravity (eq. 5.5)? Without that, it is tough to get a feel for the importance of the numbers in Table 5.3.

3c (tangential but related)
Please could there be a little discussion on the practical feasibility of controlling \delta{T} and \delta{p} such that one can measure \delta\phi_{GRAVITES} with sensible uncertainty?

3d (another tangent)
I would also like to see a discussion of the practical feasibility of controlling vertical vs horizontal gradients of T and p. For the purposes of Section 2, 3 and 4's analysis, T is taken as constant. Yet in Section 5 it is allowed to vary vertically so as to be different for each arm. But if T is constant along the fibre, then in real life it must also be constant along the spool -- and that would seem to rule out vertical gradients. Essentially we seem to require that the temperature not vary vertically along the length scale of the spool, but that it potentially vary vertically between the interferometer's arms. Is this a contradiction? In this connection, it would be nice to know roughly how tall the spools will be.

4
Miscellaneous

4a
I do not agree that ``[l]arge elastic deformations of gravitating cylindrical bodies play a significant role in everyday life". Spherical bodies, yes. But cylindrical ones... surely not?! Is it simply a misprint, with the authors actually wishing to state the opposite? That would make better sense to me, given that the following sentence starts by drawing a contrast (``On the other hand [...]"). Whatever the case, I really think that this first sentence must be changed or removed.

4b
It is not (necessarily) the problem of these authors, but does Fig. 1.1 really need that background that seems to be representing curved spacetime? It makes the cartoon rather hard to read. How are the two spools distributed in space with respect to each other? A background that helps to show that distribution would be much more helpful, at least to me.

4c
In fact, Figure 1.1 is not particularly helpful on its own. It is appealing as a cartoon visualising GRAVITES, but I would also appreciate a proper diagram that shows the effective setup analysed within the paper. That is, I would like to see two parallel lines whose spacing is clearly indicated, each of which has its own environmental parameters (p, T, g) associated with it, with coordinate

systems fully marked etc.

4d
Very last paragraph:
The authors state that the centrifuge setup would require a more precise model. Perhaps they could outline what aspects of the present paper's analysis would need to be changed in that case? In particular, would it still be reasonable to assume a certain along-fibre deformation and then take all other fields to depend only on coordinates tangential to the fibre?

CONCLUSION

I will be glad to see this interesting paper (and its promised follow-up!) accepted for official approval subject to dealing with the points discussed above.

Is the work clearly and accurately presented and does it cite the current literature?
Partly

Is the study design appropriate and does the work have academic merit?
Yes

Are sufficient details of methods and analysis provided to allow replication by others?
Yes

If applicable, is the statistical analysis and its interpretation appropriate?
Not applicable

Are all the source data underlying the results available to ensure full reproducibility?
No source data required

Are the conclusions drawn adequately supported by the results?
Yes

Competing Interests: No competing interests were disclosed.

Reviewer Expertise: Theoretical continuum mechanics; theoretical seismology

I confirm that I have read this submission and believe that I have an appropriate level of expertise to confirm that it is of an acceptable scientific standard, however I have significant reservations, as outlined above.

Author Response 28 Oct 2024
Elisabeth Steininger

We are grateful to the referee for his careful reading of our paper, and for helpful suggestions which led to significant improvements of our manuscript. We address the changes made in response to the comments (reproduced in italics) point by point:

1) *Please lead the reader more clearly through the analysis, stating clearly why certain equations are being derived and certain assumptions made:*
Author response: We have tried to address this in our corrections, detailed below, and in several comments added in the text.

1a) *As discussed above (and hopefully my interpretation is correct) the crucial relationship derived in the paper is eq.(3.17). But the authors do not flag the importance of this relationship explicitly, nor is eq.(3.17) even *referenced* in Section 5 when the GRAVITES estimates are made! Please make sure that this equation's importance is emphasized, and that its centrality to equations (5.1),(5.2),(5.3) -- and thus to the whole paper -- is stated.*
Author response: We have emphasized the importance of eq. (3.17) further in the text and added a reference to it for eq. (5.3).

1b) *In that connection, please make EXPLICIT that Table 5.3 refers to DIFFERENCES BETWEEN THE RESPECTIVE INTERFEROMETER ARMS. It might be obvious after a few readings of the paper -- and I have little doubt that it is trivial to people who have immersed themselves in this topic for months -- but I don't think that the present manuscript makes clear what is being compared to what. I would appreciate something like the following to be added to the end of Section 3, after eq (3.17): "Given a spooling force and upon specifying ambient gravity, pressure and temperature, eq.(3.17) allows the computation of the elongation of an optical fiber , that is of each arm of the interferometer. Now, due to the arms' one-metre vertical spacing, the ambient variables could be different for each arm; the spooling force could be different too because two different spools will be used. We should therefore expect each arm of the interferometer to be of different length. This difference in length will lead to an extra phase-shift that must be corrected for and that is derived directly from eq.(3.17). In Section 4 we proceed to derive expressions for σ_{xx} and σ_{yy} in terms of ambient pressure and gravity, so that eq.(3.17) can indeed be seen to express a relationship between each arm's actual length and: p,T,g and F_T." If words to this effect had been included in the manuscript (perhaps even in the Introduction) I think I would have had a *much* easier time understanding where things were going.*
Author response: Added some clarification following eq. (3.17) as to the relation with the following section.
Additionally added a short remark before eq. (5.1) and in the caption to clarify that we are interested in differences of configurations for the GRAVITES experiment, emphasizing that we compare two fibers with some vertical separation.
Added in the introduction a paragraph in the spirit suggested.

1c.i) *Please introduce and describe the spooling force F_T earlier in the main text, rather than just mentioning it in passing in the caption of Figure 2.1c. Preferably, state at the beginning of Section 2 that the model of the waveguide that this paper analyses in detail is the version from Figure 2.1c, and that we therefore have displacement-free boundary conditions on one end while needing to match the stress at the other end to the externally imposed force F_T. Incidentally, this would give a much clearer motivation for imposing eq.(2.5) than what the manuscript offers at present.*

Author response: Added some explanation for F_T to the caption of Figure 2.1, with reference to Section 3 where it is thoroughly discussed.
Further added some comments in the main text.
Note that the analysis in our work can be applied to any of the configurations pictured in Figure 2.1.

1c.ii) *Incidentally, this would give a much clearer motivation for imposing eq.(2.5) than what the manuscript offers at present.*
Author response: Equation (2.5) ((2.6) in the revised version) is unavoidable if one wants to take into account the three-dimensional Poisson effect, while remaining compatible with a basically 2-dimensional description used in our calculation.

1d.i) *Following on directly from 1c, please motivate eq.(2.5) more clearly (I didn't find the statement "compare Figure 2.1 (a)–(c)" to help much in that regard). Once the spooling force has been foregrounded, this should be easy.*
Author response: (Hopefully this has been taken care of by our previous additions)

1d.ii) *In addition, I would appreciate a note after eq.(2.10) stating that the z-component of the force-balance equation is automatically satisfied.*
Author response: Comment added.

1e.i) *Eq.(2.1): What are σ and ϵ?! A reader without much background in elasticity would be stuck here; please define all terms used in the paper. In addition, eq.(2.6) should logically precede eq.(2.1): how can you define strain without any concept of deformation? Also, the material need not be homogeneous for eq.(2.1) to hold.*
Author response: Text rearranged, defined the stress and strain tensors in the text.
Added a comment that we restrict to constant material parameters and thus homogeneous materials.

1e.ii) *Eq. (2.11): $\sigma_{rr} + \sigma_{\theta\theta}$ should probably read $\sigma_{xx} + \sigma_{yy}$ because the cylindrical coordinate system has not yet been introduced.*
Author response: Fixed.

1e.iii) *Eq.(4.32): Please define both `A' and the concept of `indicator function'. (Presumably A here is different from the A in equations (4.10), (4.11) and (4.12)?!)* Changed the previous symbol A to Ω to make clear that there is no relation to Eq. (4.10)-(4.12).
Author response: Removed the notion `indicator function'.

1e.iv) *Eq.(5.3): ⬚⬚$\sigma_{\theta\theta}$ has not yet been formally defined. Eq.(5.1) should be adjusted to include this definition.*
Author response: Added a reference to ⬚⬚$\sigma_{\theta\theta}$.

2) *Temperature and thermo-elasticity. A temperature T_0 is introduced in eq.(2.3) as a `baseline', with T being the actual (constant) temperature of the optical fiber . Assuming that ⬚⬚T in Table 5.3 represents the difference between the *actual* temperatures of the interferometer's respective arms, then eq.(5.3) should have ($T-T_0$) replaced by ⬚⬚T. (This caused me a lot of confusion at first!)*

Author response: Fixed.

3) *I would like to see more uncertainty estimates, please.*
Author response: Added.

3a) *What is the rough uncertainty on the spooling force. How different will it therefore be between the two arms?* Added the uncertainty.
Author response: Added an explanation that we assume that the forces in both arms are the same and that they do not change when an arm is moved in the gravitational field.

3b) *What is the rough uncertainty on phase-shift due to gravity (eq. 5.5)? Without that, it is tough to get a feel for the importance of the numbers in Table 5.3.*
Author response: Added (expected accuracy is 95%).

3c) *(tangential but related) Please could there be a little discussion on the practical feasibility of controlling ��T and ��p such that one can measure ��$\phi_{GRAVITES}$ with sensible uncertainty?*
Author response: Comments added.

3d) *I would also like to see a discussion of the practical feasibility of controlling vertical vs horizontal gradients of T and p. For the purposes of Section 2, 3 and 4's analysis, T is taken as constant. Yet in Section 5 it is allowed to vary vertically so as to be different for each arm. But if T is constant along the fiber , then in real life it must also be constant along the spool -- and that would seem to rule out vertical gradients. Essentially we seem to require that the temperature not vary vertically along the length scale of the spool, but that it potentially vary vertically between the interferometer's arms. Is this a contradiction? In this connection, it would be nice to know roughly how tall the spools will be.*
Author response: Comments added: the spools are expected to be of the order of 30 cm, so there will be a gradient which will have a nontrivial effect on each arm. But in GRAVITES what matters is not the geometry but its change when the arm is moved up, therefore we expect that our model should suffice to give a good estimates of the effects on GRAVITES. One way of mitigating the results of the deformations predicted by our calculations will be to place each arm in a separate vacuum chamber. This is one of the configurations that is being explored now.

4a) *I do not agree that ``[l]arge elastic deformations of gravitating cylindrical bodies play a significant role in everyday life". Spherical bodies, yes. But cylindrical ones... surely not?! Is it simply a misprint, with the authors actually wishing to state the opposite? That would make better sense to me, given that the following sentence starts by drawing a contrast (``On the other hand [...]"). Whatever the case, I really think that this first sentence must be changed or removed.*
Author response: Sentence removed.

4b) *It is not (necessarily) the problem of these authors, but does Fig. 1.1 really need that background that seems to be representing curved spacetime? It makes the cartoon rather hard to read. How are the two spools distributed in space with respect to each other? A background that helps to show that distribution would be much more helpful, at least to me.* **Author response:** Added a comment regarding the background of Fig. 1.1 in its caption and expanded on the description.

4c) *In fact, Figure 1.1 is not particularly helpful on its own. It is appealing as a cartoon visualising GRAVITES, but I would also appreciate a proper diagram that shows the effective setup analysed within the paper. That is, I would like to see two parallel lines whose spacing is clearly indicated, each of which has its own environmental parameters (p, T, g) associated with it, with coordinate systems fully marked etc.*
Author response: Figure revised, and a second figure added.

4d) *Very last paragraph: The authors state that the centrifuge setup would require a more precise model. Perhaps they could outline what aspects of the present paper's analysis would need to be changed in that case? In particular, would it still be reasonable to assume a certain along-fiber deformation and then take all other fields to depend only on coordinates tangential to the fiber?*
Author response: Some comments added.

Competing Interests: No competing interests were disclosed.

Reviewer Report 19 July 2024

https://doi.org/10.21956/openreseurope.18729.r41517

© 2024 Beig R. This is an open access peer review report distributed under the terms of the Creative Commons Attribution License, which permits unrestricted use, distribution, and reproduction in any medium, provided the original work is properly cited.

Robert Beig
[1] Gravitational Physics/Physics Faculty, Universitat Wien, Vienna, Austria
[2] Gravitational Physics/Physics Faculty, Universitat Wien, Vienna, Austria

An experiment is currently developed aiming at measuring the influence of gravity on entangled states of photons in an optical fiber. Gravity will also deform the shape of the waveguide, which potentially changes the phase shift to be measured in the experiment. The paper by Barzegar .,et al calculates these elastic deformations, using linearized (thermo-) elasticity for isotropic, homogenous materials - which should be a valid approximation under present circumstances. The main issue in their calculations comes from boundary conditions at the rigid plane where the cylindrical wave guide is placed. In a first step the authors assume this contact to occur across a line. The results in that case, as the authors point out, and as is known from the literature they cite, is 'unphysical' - by which they mean that the obtained deformation diverges at the contact interfaces. In a second part the authors improve these solutions by employing Hertz-type boundary conditions at these interfaces. Finally, in section 5, the authors, estimate the influence on elastic deformations on the planned GRAVITES experiment. They expect this influence on the measured phase shift to be 2 orders of magnitude smaller than that due to electromagnetism. More details are promised from electromagnetic calculations under way.
I find the topic of this paper timely. The paper is well written, Without having checked details, I expect the calculations to be correct.
I would like to raise one point concerning the presentation. Due to symmetry the work in this

paper takes place in 2d. Here, if the external force field. Comes from a potential which is harmonic (as to good approximation is the case for terrestrial gravity) and temperature is constant, the field equations boil down to the biharmonic equation for a scalar called an Airy function in the literature plus suitable boundary conditions. (One can then use an explicit expression for the general solution to the latter equation, Fourier expanded with respect to angle, known as the Michell solution in the literature.) It would greatly benefit a general theoretical physics audience if the authors cared to spend a few lines explaining the process leading from the standard field equations to the biharmonic equation rather than only referring to the classical, engineering-type literature. The basic observation (apparently due to Airy) is that a divergence-free symmetric tensor in 2d can be written as.
$\sigma_{ij} = \varepsilon_{ij} \Delta\Phi - \partial_i \partial_J \Phi$
The authors might also mention that the 'compatibility condition' leading from there to the biharmonic equation is actually a purely geometric condition on a symmetric tensor in order to be the linearized strain tensor of a deformation.

Is the work clearly and accurately presented and does it cite the current literature?
Yes

Is the study design appropriate and does the work have academic merit?
Yes

Are sufficient details of methods and analysis provided to allow replication by others?
Yes

If applicable, is the statistical analysis and its interpretation appropriate?
Not applicable

Are all the source data underlying the results available to ensure full reproducibility?
Yes

Are the conclusions drawn adequately supported by the results?
Yes

Competing Interests: No competing interests were disclosed.

Reviewer Expertise: General Relativity, Relativistic Elasticity

I confirm that I have read this submission and believe that I have an appropriate level of expertise to confirm that it is of an acceptable scientific standard.

Author Response 28 Oct 2024

Elisabeth Steininger

We are grateful to the referee for his careful reading of our paper, and for helpful suggestions which led to significant improvements of our manuscript. We address the changes made in the revision as a response to the comments (reproduced in italics) point by

point:

- *It would greatly benefit a general theoretical physics audience if the authors cared to spend a few lines explaining the process leading from the standard field equations to the biharmonic equation rather than only referring to the classical, engineering-type literature. The basic observation (apparently due to Airy) is that a divergence-free symmetric tensor in 2d can be written as* $\sigma ij = {}^{\delta}ij\ \Delta\Phi - \partial i \partial j\Phi$.

We added the geometric version of the equation defining the Airy stress function, to make the manuscript easier to read, with suitable comments.

- *The authors might also mention that the 'compatibility condition' leading from there to the biharmonic equation is actually a purely geometric condition on a symmetric tensor in order to be the linearized strain tensor of a deformation.*

It is our understanding that the referee meant that the "compatibility condition" for the Airy stress function is a geometric condition related to the vanishing, in the linear regime, of the Riemann tensor of the pullback of the metric from the spacetime manifold to the body manifold. We have added references to the literature on the subject in the introduction, but explaining all this might create confusion, as this is not necessary in our context.

Competing Interests: No competing interests were disclosed.